

# Implementation of the HMC algorithm on the tempered Lefschetz thimble method

Masafumi Fukuma<sup>1\*</sup>, Nobuyuki Matsumoto<sup>1†</sup> and Naoya Umeda<sup>2‡</sup>

<sup>1</sup>*Department of Physics, Kyoto University, Kyoto 606-8502, Japan*

<sup>2</sup>*PricewaterhouseCoopers Aarata LLC,*

*Otemachi Park Building, 1-1-1 Otemachi, Chiyoda-ku, Tokyo 100-0004, Japan*

## Abstract

The tempered Lefschetz thimble method (TLTM) is a parallel tempering algorithm towards solving the numerical sign problem, where the system is tempered by the antiholomorphic gradient flow to tame both the sign and ergodicity problems simultaneously. In this paper, we implement the hybrid Monte Carlo (HMC) algorithm for transitions on each flowed surface, expecting that this implementation on TLTM will give a useful framework for future computations on large-scale systems including fermions. Although the use of HMC in Lefschetz thimble methods has been proposed so far, our crucial achievements here are two-fold: One is the development of a molecular dynamics algorithm to correctly sample configurations near zeros of fermion determinants. The other is the implementation of HMC so as to work within the parallel tempering algorithm in TLTM. We confirm that the algorithm works correctly by applying it to the sign problem of the Hubbard model on a small lattice, for which the TLTM is known to work with the Metropolis algorithm. We show that the use of HMC significantly reduces the autocorrelation times with less computational times compared to the Metropolis algorithm.

---

\*E-mail address: fukuma@gauge.scphys.kyoto-u.ac.jp

†E-mail address: nobu.m@gauge.scphys.kyoto-u.ac.jp

‡E-mail address: n.umedo@gauge.scphys.kyoto-u.ac.jp

# Contents

<b>1</b>	<b>Introduction</b>	<b>1</b>
<b>2</b>	<b>Preparations</b>	<b>3</b>
2.1	Tempered Lefschetz thimble method (review) . . . . .	3
2.2	Real representation for complex variables . . . . .	5
2.3	Overview of the implementation of HMC on TLTM . . . . .	5
<b>3</b>	<b>Molecular dynamics on flowed surfaces</b>	<b>7</b>
3.1	Molecular dynamics on a general constrained surface . . . . .	7
3.2	Molecular dynamics on a flowed surface $\Sigma_t$ . . . . .	10
<b>4</b>	<b>HMC on TLTM</b>	<b>14</b>
4.1	Swap of configurations at adjacent replicas . . . . .	15
4.2	Summary of HMC on TLTM . . . . .	16
<b>5</b>	<b>Results and analysis</b>	<b>18</b>
5.1	Hubbard model and the parameters for simulations . . . . .	18
5.2	Estimate of the number density . . . . .	20
5.3	Autocorrelations . . . . .	21
<b>6</b>	<b>Conclusion and outlook</b>	<b>25</b>

## 1. Introduction

The Markov chain Monte Carlo (MCMC) method has been an important tool in theoretical physics as it enables nonperturbative calculations of physical quantities. However, its application to some important research areas in physics is still hindered due to the numerical *sign problem*. Examples include finite density QCD [1], the quantum Monte Carlo simulations of strongly correlated electron systems [2, 3], and real-time quantum field theories. Among many approaches towards solving the sign problem, algorithms using Lefschetz thimbles [4, 5, 6, 7, 8, 9, 10, 11, 12] have been developed because of its mathematical rigor [13]. Along the line of such developments, the *tempered Lefschetz thimble method* (TLTM) was proposed [11, 12] as a versatile solution to the sign problem.<sup>1</sup>

---

<sup>1</sup>See [14] for a similar idea.

As will be reviewed in the next section, the TLTM is a parallel-tempering algorithm, where the tempering parameter is set to be the flow time of the antiholomorphic gradient flow. This is to resolve the dilemma between the sign and ergodicity problems that becomes manifest when contributions from multiple thimbles are relevant. The validity of TLTM has been confirmed for various models, including the  $(0+1)$ -dimensional massive Thirring model [11], the Hubbard model away from half filling [12] and a class of chiral matrix models (to be reported in another communication).

As an algorithm to generate transitions on each flowed surface in TLTM, we have adopted the Metropolis algorithm in our previous study because of its simplicity. However, it is known that the Metropolis algorithm becomes less efficient than the Hybrid Monte Carlo (HMC) algorithm for systems including fermions with large degrees of freedom [15, 16]. Thus, the implementation of HMC on TLTM must give a useful framework for future computations on large-scale systems including fermions.

Our implementation of HMC on TLTM is based on the RATTLE algorithm [17, 18] for molecular dynamics on flowed surfaces. The use of RATTLE in Lefschetz thimble methods has already been considered by several groups [7, 19]. Our crucial achievements here are two-fold: One is the development of a molecular dynamics algorithm to correctly sample configurations near zeros of fermion determinants.<sup>2</sup> The other is the implementation of HMC so as to work within the parallel tempering algorithm in TLTM. To demonstrate that the implementation works correctly with high efficiency, we apply it to the Hubbard model away from half filling with small degrees of freedom ( $N = 20$  for an  $N_s = 2 \times 2$  spatial lattice with  $N_\tau = 5$  imaginary time steps), for which the TLTM is known to work correctly with the Metropolis algorithm [12].<sup>3</sup> We show that our new algorithm gives results that agree nicely with exact values, and the computational cost to obtain an independent configuration is reduced to about 30% of that of the Metropolis algorithm. We expect that greater efficiency will be gained for larger degrees of freedom.

This paper is organized as follows. In section 2, we first review the basics of the TLTM. Then, after a short explanation on our convention, we give an overview on the implementation of HMC on the TLTM. We in section 3 explain a general theory for molecular dynamics on flowed surfaces, and in section 4 give the explicit algorithm to implement HMC on the TLTM. The algorithm is applied to the Hubbard model in section 5, and is shown to work correctly with reduced computational costs compared with the Metropolis algorithm. Section 6 is devoted to conclusion and outlook.

---

<sup>2</sup>This is necessary because configurations around zeros (in complex space  $\mathbb{C}^N$ ) are reached with finite flow times and can be relevant to observables under consideration.

<sup>3</sup>See [20, 21, 22, 23] for related work on the application of Lefschetz thimble methods to the Hubbard model.

## 2. Preparations

In this section, we first review the basics of TLTM. Then, after a short explanation on our convention, we give an overview on the implementation of HMC on TLTM.

### 2.1. Tempered Lefschetz thimble method (review)

Let  $\mathbb{R}^N = \{x\}$  be a configuration space of  $N$ -dimensional real variable  $x = (x^i)$  ( $i = 1, \dots, N$ ), and  $S(x)$  the action. Our main concern is to estimate the expectation value of an observable  $\mathcal{O}(x)$ ,

$$\langle \mathcal{O}(x) \rangle \equiv \frac{\int_{\mathbb{R}^N} dx e^{-S(x)} \mathcal{O}(x)}{\int_{\mathbb{R}^N} dx e^{-S(x)}}. \quad (2.1)$$

In this paper, we always assume that both  $e^{-S(z)}$  and  $e^{-S(z)} \mathcal{O}(z)$  are entire functions over  $\mathbb{C}^N$ . We further assume that there is no multimodal problem on the original configuration space  $\mathbb{R}^N$  ( $\subset \mathbb{C}^N$ ) with respect to  $\text{Re } S(x)$ . Then, due to Cauchy's theorem in higher dimensions, the first assumption ensures that the integrals in (2.1) do not change under continuous deformations of the integration region from  $\mathbb{R}^N$  to  $\Sigma$  with the boundary at  $|x| \rightarrow \infty$  kept fixed:

$$\langle \mathcal{O}(x) \rangle = \frac{\int_{\Sigma} dz e^{-S(z)} \mathcal{O}(z)}{\int_{\Sigma} dz e^{-S(z)}}. \quad (2.2)$$

The sign problem will then get much reduced if  $\text{Im } S(z)$  is almost constant on  $\Sigma$ .

The Markov chain Monte Carlo (MCMC) calculation of (2.2) can be performed as follows. First, we decompose the complex measure  $dz \equiv \prod_{i=1}^N dz^i$  to the modulus  $|dz|$  and the phase  $e^{i\varphi(z)}$ ,

$$dz = |dz| e^{i\varphi(z)}, \quad (2.3)$$

and rewrite  $dz e^{-S(z)}$  as<sup>4</sup>

$$dz e^{-S(z)} = |dz| e^{-\text{Re } S(z)} e^{i\theta(z)} \quad (e^{i\theta(z)} \equiv e^{i\varphi(z)} e^{-i\text{Im } S(z)}), \quad (2.4)$$

from which (2.2) will be written as a ratio of reweighted integrals on  $\Sigma$ :

$$\langle \mathcal{O}(x) \rangle = \frac{\int_{\Sigma} dz e^{-S(z)} \mathcal{O}(z)}{\int_{\Sigma} dz e^{-S(z)}} = \frac{\langle e^{i\theta(z)} \mathcal{O}(z) \rangle_{\Sigma}}{\langle e^{i\theta(z)} \rangle_{\Sigma}} \quad (2.5)$$

with

$$\langle f(z) \rangle_{\Sigma} \equiv \frac{1}{Z} \int_{\Sigma} |dz| e^{-\text{Re } S(z)} f(z) \quad (Z = \int_{\Sigma} |dz| e^{-\text{Re } S(z)}). \quad (2.6)$$

---

<sup>4</sup>Note that  $|dz|$  agrees with the volume element associated with the induced metric on  $\Sigma$  in  $\mathbb{R}^{2N}$  ( $= \mathbb{C}^N$ ).

We then generate a sample  $\{z^{(k)}\}_{k=1,\dots,N_{\text{conf}}}$  from the distribution  $e^{-\text{Re } S(z)}/Z$ , and estimate  $\langle f(z) \rangle_\Sigma$  as a sample average

$$\langle f(z) \rangle_\Sigma \approx \frac{1}{N_{\text{conf}}} \sum_{k=1}^{N_{\text{conf}}} f(z^{(k)}) \equiv \overline{f(z)}, \quad (2.7)$$

from which  $\langle \mathcal{O}(x) \rangle$  is estimated as<sup>5</sup>

$$\langle \mathcal{O}(x) \rangle = \frac{\langle e^{i\theta(z)} \mathcal{O}(z) \rangle_\Sigma}{\langle e^{i\theta(z)} \rangle_\Sigma} \approx \frac{\overline{e^{i\theta(z)} \mathcal{O}(z)}}{\overline{e^{i\theta(z)}}} \equiv \bar{\mathcal{O}}. \quad (2.8)$$

In a class of Lefschetz thimble methods (see, e.g., [9, 10, 11, 12]), continuous deformations of integration region are made according to the antiholomorphic flow equation:

$$\dot{z}_t^i = [\partial_i S(z_t)]^*, \quad z_{t=0}^i = x^i. \quad (2.9)$$

Since  $(d/dt) S(z_t) = |\partial_i S(z_t)|^2 \geq 0$ , the real part  $\text{Re } S(z_t)$  always increase along the flow except at critical points  $z_\sigma$  (where  $\partial_i S(z_\sigma) = 0$ ), while the imaginary part  $\text{Im } S(z_t)$  is kept constant. In the limit  $t \rightarrow \infty$ ,  $\Sigma_t \equiv z_t(\mathbb{R}^N)$  will approach a union of Lefschetz thimbles, on each of which  $\text{Im } S(z)$  is constant, and thus the sign problem is expected to disappear there (except for a possible residual and/or global sign problem).<sup>6</sup> However, for large  $t$  there arises a new problem, multimodal (ergodicity) problem, because the potential barriers between different thimbles become infinitely high as  $t$  increases.

In the tempered Lefschetz thimble method (TLTM) [11, 12], we resolve the dilemma between the sign problem (severe at small flow times) and the ergodicity problem (severe at large flow times) by tempering the system with the flow time.<sup>7</sup> The algorithm consists of three steps. (1) First, we introduce a set of configuration spaces,  $\{\Sigma_{t_a}\}$  ( $a = 0, 1, \dots, A$ ), with  $t_0 = 0 < t_1 < \dots < t_A = T$ . We often call  $\Sigma_{t_a}$  the  $a$ -th replica. Here, a possible criterion for choosing the maximum flow time  $T$  is that the sign average  $|\langle e^{i\theta(z)} \rangle_{\Sigma_T}|$  is  $O(1)$  without tempering. (2) We then construct a Markov chain that drives the enlarged system  $\Sigma_{\text{tot}} \equiv \Sigma_{t_0} \times \Sigma_{t_1} \times \dots \times \Sigma_{t_A} = \{\vec{z} = (z_a)\}$  to global equilibrium with the distribution  $p_{\text{eq}}(\vec{z}) \propto \prod_a \exp[-\text{Re } S(z_a)]$ . (3) After the system is well relaxed to global equilibrium, we estimate the expectation value on  $\Sigma_{t_a}$  [see (2.8)] by using the subsample at replica  $a$ ,  $\{z_a^{(k)}\}_{k=1,2,\dots,N_{\text{conf}}}$ , that is retrieved from the total sample  $\{\vec{z}^{(k)} = (z_0^{(k)}, z_1^{(k)}, \dots, z_A^{(k)})\}_{k=1,2,\dots,N_{\text{conf}}}$ :

$$\frac{\langle e^{i\theta(z_a)} \mathcal{O}(z_a) \rangle_{\Sigma_{t_a}}}{\langle e^{i\theta(z_a)} \rangle_{\Sigma_{t_a}}} \approx \frac{\overline{e^{i\theta(z_a)} \mathcal{O}(z_a)}}{\overline{e^{i\theta(z_a)}}} \equiv \bar{\mathcal{O}}_a. \quad (2.10)$$

---

<sup>5</sup>The statistical error of  $\langle f(z) \rangle_\Sigma$  as well as that of the ratio  $\bar{\mathcal{O}}$  will be estimated from the Jackknife method with bins (by taking account of autocorrelations).

<sup>6</sup>In the case when the action diverges at some points in  $\mathbb{C}^N$  (such as zeros of the fermion determinant),  $\Sigma_t$  should be understood to represent  $z_t(\mathbb{R}^N)$  with these points removed.

<sup>7</sup>As a tempering algorithm, we adopt the parallel tempering (also called the replica exchange MCMC method) [24, 25, 26] because then we need not specify the probability weight factors at various flow times and because most of relevant steps can be done in parallel processes.

Since the left-hand side of (2.10) is independent of  $a$  due to Cauchy's theorem, the ratio  $\bar{\mathcal{O}}_a$  at large  $a$ 's (where the sign problem is relaxed) should yield the same value within the statistical error margin if the system is well in global equilibrium. Conversely, the requirement of  $a$ -independence ensures the sample to be in global equilibrium with a sufficient sample size (together with the correctness of the employed numerical method), and is the basis of the following algorithm for precise estimation [12]. First, we continue the sampling until we find some range of  $a$ , in which  $|\overline{e^{i\theta(z_a)}}|$  are well above  $1/\sqrt{2N_{\text{conf}}}$  (the values for the uniform distribution of phases) and  $\bar{\mathcal{O}}_a$  take the same value within the statistical error margin. Then, we estimate  $\langle \mathcal{O} \rangle$  by using the  $\chi^2$  fit (using covariance) of  $\{\bar{\mathcal{O}}_a\}$  in this region with a constant function of  $a$ . Global equilibrium and the sufficiency of the sample size are checked by looking at the optimized value of  $\chi^2/\text{DOF}$ .

## 2.2. Real representation for complex variables

In the following sections, we mainly use the real representation for complex variables, where a point  $z = (z^i) = x + iy \in \mathbb{C}^N$  ( $i = 1, \dots, N$ ) is expressed by  $z = (z^I) \equiv (x, y)^T \in \mathbb{R}^{2N}$  ( $I = 1, \dots, 2N$ ). Accordingly, a complex column vector  $v = (v^i) = v_R + iv_I \in \mathbb{C}^N$  will be written as a real vector  $v = (v^I) \equiv (v_R, v_I)^T \in \mathbb{R}^{2N}$ . Under this identification, an  $N \times N$  complex matrix  $A = (A_{ij}) = A_R + iA_I$  will be given as a  $2N \times 2N$  matrix,

$$A = (A_{IJ}) \equiv \begin{pmatrix} A_R & -A_I \\ A_I & A_R \end{pmatrix}. \quad (2.11)$$

We write the multiplication of  $i$  (imaginary unit) and the complex conjugation, respectively, as

$$\hat{i} \equiv \begin{pmatrix} 0 & -1_N \\ 1_N & 0 \end{pmatrix}, \quad \hat{C} \equiv \begin{pmatrix} 1_N & 0 \\ 0 & -1_N \end{pmatrix}, \quad (2.12)$$

and introduce the projectors to the real and imaginary parts, respectively, as

$$\widehat{\text{Re}} \equiv \frac{1}{2} (1 + \hat{C}) = \begin{pmatrix} 1_N & 0 \\ 0 & 0 \end{pmatrix}, \quad \widehat{\text{Im}} \equiv \frac{1}{2} (1 - \hat{C}) = \begin{pmatrix} 0 & 0 \\ 0 & 1_N \end{pmatrix}. \quad (2.13)$$

## 2.3. Overview of the implementation of HMC on TLTM

We will often abbreviate flowed surfaces  $\Sigma_{t_a} = \{z_a\}$  as  $\Sigma_a$  ( $a = 0, 1, \dots, A$ ) to simplify expressions. In the parallel tempering, the total configuration space is given by

$$\Sigma_{\text{tot}} \equiv \Sigma_0 \times \dots \times \Sigma_A = \{\vec{z} = (z_a)\}, \quad (2.14)$$

which we regard as a complex of playgrounds with  $A + 1$  zones for the same number of molecules, where each molecule moves around from a zone to another zone under the condition that any two molecules cannot be in the same zone.<sup>8</sup> In order to implement an HMC algorithm on the tempered system, we introduce to each replica  $\Sigma_a$  the phase space  $T^*\Sigma_a = \{\zeta_a = (z_a, \pi_a)\}$  and the Hamiltonian

$$H_a(\zeta_a) \equiv \frac{\pi_a^2}{2M_a} + V(z_a), \quad (2.15)$$

where  $\pi_a^2/2M_a \equiv (1/2)(M_a^{-1})^{IJ}\pi_{a,I}\pi_{a,J}$  and  $V(z_a) \equiv \text{Re } S(z_a)$ .  $M_a$  is constant and will be set to be  $(M_a)_{IJ} = \sigma_a^2 \delta_{IJ}$ .

We construct a molecular dynamics on each phase space  $T^*\Sigma_a$  (to be explained in detail in the next section), that defines a one-body motion from  $\zeta_a \in T^*\Sigma_a$  to  $\zeta'_a \equiv \Phi_a(\zeta_a) \in T^*\Sigma_a$ .  $\Phi_a$  will be designed such that it is volume-preserving and reversible, and thus the transition probability<sup>9</sup>

$$\mathbb{P}_a^{(1)}(\zeta'_a|\zeta_a) \equiv \min\left(1, e^{-H_a(\zeta'_a) + H_a(\zeta_a)}\right) \delta(\zeta'_a - \Phi_a(\zeta_a)) \quad (\zeta'_a \neq \zeta_a) \quad (2.16)$$

satisfies the relation

$$\mathbb{P}_a^{(1)}(\zeta'_a|\zeta_a) e^{-H_a(\zeta_a)} = \mathbb{P}_a^{(1)}(\zeta_a^T|\zeta_a'^T) e^{-H_a(\zeta_a')}, \quad (2.17)$$

where  $\zeta^T \equiv (z, -\pi)$  for  $\zeta = (z, \pi)$  and we have used the fact  $H_a(\zeta_a^T) = H_a(\zeta_a)$ .

We then define a transition probability on each replica:<sup>10</sup>

$$P_a^{(1)}(z'_a|z_a) \equiv c_a \int d\pi'_a d\pi_a \mathbb{P}_a^{(1)}(z'_a, \pi'_a|z_a, \pi_a) e^{-\pi_a^2/2M_a} \quad (2.18)$$

with  $c_a \equiv [\int d\pi_a e^{-\pi_a^2/2M_a}]^{-1}$ .  $P_a^{(1)}$  satisfies the following detailed balance condition:

$$P_a^{(1)}(z'_a|z_a) e^{-V(z_a)} = P_a^{(1)}(z_a|z'_a) e^{-V(z'_a)}. \quad (2.19)$$

We also introduce a two-body evolution that maps  $(z_a, z_b) \in \Sigma_a \times \Sigma_b$  to  $(z'_a, z'_b) \in \Sigma_a \times \Sigma_b$  with the probability  $P_{ab}^{(2)}(z'_a, z'_b|z_a, z_b)$  that satisfies the relation

$$P_{ab}^{(2)}(z'_a, z'_b|z_a, z_b) e^{-V(z_a) - V(z_b)} = P_{ab}^{(2)}(z_a, z_b|z'_a, z'_b) e^{-V(z'_a) - V(z'_b)}. \quad (2.20)$$

By combining  $P_a^{(1)}$  and  $P_{ab}^{(2)}$ , one can construct a Markov chain such that its transition probability  $P_{\text{tot}}(\vec{z}'|\vec{z})$  gives the desired equilibrium distribution  $p_{\text{eq}}(\vec{z}) \propto \prod_a e^{-V(z_a)}$ .

In the following sections, we define a molecular dynamics on each replica (section 3) and then give an explicit algorithm for HMC on TLTM (section 4).

<sup>8</sup> Note that the index  $a$  labels the zones, not the molecules.

<sup>9</sup>The diagonal elements are determined automatically by the probability conservation  $\int d\zeta'_a \mathbb{P}_a^{(1)}(\zeta'_a|\zeta_a) = 1$ . This comment will be applied to similar expressions in what follow.

<sup>10</sup> $d\pi_a$  is the volume element of  $T_{z_a}^*\Sigma_a$  and will be denoted by  $(d\pi_a)_\parallel$  when  $\pi_a$  is an element in  $T_{z_a}^*\mathbb{R}^{2N}$ .

### 3. Molecular dynamics on flowed surfaces

In this section, we first give a brief review of molecular dynamics on a general constrained surface  $\Sigma$ , and then discuss molecular dynamics on a flowed surface  $\Sigma = \Sigma_t$  that is obtained as a time slice from the antiholomorphic gradient flow with flow time  $t$ .

#### 3.1. Molecular dynamics on a general constrained surface

Let  $\Sigma$  be an  $m$ -dimensional surface in  $\mathbb{R}^{2N}$  ( $= \mathbb{C}^N$ ), which we assume is given by a set of constraint equations<sup>11</sup>

$$\phi^r(z) = 0 \quad (r = 1, \dots, 2N - m). \quad (3.1)$$

At point  $z \in \Sigma$ , we choose a basis of the tangent space  $T_z\Sigma$  and denote it by  $E_\alpha = (E_\alpha^I)$  ( $\alpha = 1, \dots, m$ ), from which we define the metric  $g_{\alpha\beta} \equiv \delta_{IJ} E_\alpha^I E_\beta^J$ . We also introduce a basis  $F_r = (F_r^I)$  of the normal space  $N_z\Sigma$ .

When we consider probability densities  $p(z)$  at  $z \in \Sigma$ , they are always with respect to the volume element  $|dz|$ . The volume element  $|dz|$  will also be written as  $(dz)_\parallel$  in later discussions. A transition from  $p(z)$  to  $\tilde{p}(z)$  with transition probability  $P(z'|z)$  is then expressed as

$$\tilde{p}(z') = \int_{\Sigma} |dz| P(z'|z) p(z) \quad (z' \in \Sigma). \quad (3.2)$$

Let  $T^*\mathbb{R}^{2N} = \{\zeta = (z, \pi)\}$  be the phase space on  $\mathbb{R}^{2N}$  with a separable Hamiltonian of the form

$$H(\zeta) = H(z, \pi) = \frac{1}{2} (M^{-1})^{IJ} \pi_I \pi_J + V(z), \quad (3.3)$$

where the positive symmetric mass matrix  $M = (M_{IJ})$  is assumed to be constant.<sup>12</sup> A motion on  $\Sigma$  defines a motion in the reduced phase space,

$$T^*\Sigma \equiv \{\zeta = (z, \pi) \in T^*\mathbb{R}^{2N} \mid \phi^r(z) = 0, (M^{-1}\pi)^I \partial_{z^I} \phi^r(z) = 0\}. \quad (3.4)$$

The symplectic structure of  $T^*\Sigma$  is defined by the induced symplectic form

$$\omega \equiv d\pi_I \wedge dz^I|_{T^*\Sigma}, \quad (3.5)$$

from which we define the volume element  $dV$  on  $T^*\Sigma$  by

$$dV \equiv \frac{\omega^m}{m!}. \quad (3.6)$$

---

<sup>11</sup>Later we will set  $m = N$ .

<sup>12</sup>We assume that  $M$  satisfies the condition  $M_{IJ} E_\alpha^I F_r^J = 0$ , which ensures that  $(M^{-1})^{IJ} \pi_J$  is on the tangent space  $T_z\Sigma$  for  $\pi = (\pi_I) \in T_z^*\Sigma$ .

When  $d^{2N}z \equiv \prod_I dz^I$  and  $d^{2N}\pi \equiv \prod_I d\pi_I$  are orthogonally decomposed as

$$d^{2N}z = (dz)_{\parallel} (dz)_{\perp}, \quad d^{2N}\pi = (d\pi)_{\parallel} (d\pi)_{\perp}, \quad (3.7)$$

one can easily show that

$$dV = (dz)_{\parallel} (d\pi)_{\parallel}. \quad (3.8)$$

Note that  $(dz)_{\parallel} = |dz|$  and  $(d\pi)_{\parallel}$  corresponds to  $d\pi$  in subsection 2.3. When we introduce local coordinates  $\xi = (\xi^\alpha)$  on  $\Sigma$ , then we can choose the basis of  $T_z\Sigma$  to be  $E_\alpha^I = \partial z^I / \partial \xi^\alpha$ . It is convenient to define the projected components  $\eta_\alpha$  for arbitrary momentum  $\tilde{\pi} = (\tilde{\pi}_I) \in T_z^*\mathbb{R}^{2N}$ :

$$\eta_\alpha \equiv \tilde{\pi}_I E_\alpha^I. \quad (3.9)$$

One can easily show

$$\omega = d\eta_\alpha \wedge d\xi^\alpha, \quad (3.10)$$

and thus the volume element can be expressed as<sup>13</sup>

$$dV = \prod_\alpha d\xi^\alpha d\eta_\alpha. \quad (3.11)$$

One can also show that the projection of  $\tilde{\pi}$  to  $\pi = \tilde{\pi}_{\parallel}$  is given by

$$\pi_I = \eta_\alpha E_I^\alpha = \tilde{\pi}_J \mathcal{P}_J^I, \quad (3.12)$$

where  $E_I^\alpha \equiv g^{\alpha\beta} \delta_{IJ} E_\beta^J$  [ $(g^{\alpha\beta}) \equiv (g_{\alpha\beta})^{-1}$ ] and  $\mathcal{P}_J^I \equiv E_\alpha^J E_I^\alpha$ .

In the continuous language, a motion  $\zeta(s) = (z(s), \pi(s))$  in  $T^*\Sigma$  is described by the following equations with Lagrange multipliers  $\lambda_r$ :

$$\partial_s z^I = \partial_{\pi_I} H = (M^{-1}\pi)^I, \quad (3.13)$$

$$\partial_s \pi_I = -\partial_{z^I} H - \lambda_r \partial_{z^I} \phi^r(z) = -\partial_{z^I} V(z) - \lambda_r \partial_{z^I} \phi^r(z), \quad (3.14)$$

$$0 = \phi^r(z), \quad (3.15)$$

$$0 = (M^{-1}\pi)^I \partial_{z^I} \phi^r(z). \quad (3.16)$$

Note that (3.16) (obtained by taking the derivative of (3.15) with respect to  $s$ ) means that the velocity  $\partial_s z = M^{-1}\pi$  is tangent to  $\Sigma$ . Equations (3.13)–(3.16) have the following properties: (1) symplecticity: The induced symplectic form (3.5) does not change under the motion,  $\partial_s \omega = 0$ , and thus the volume element  $dV$  is preserved. (2) reversibility: For

---

<sup>13</sup>With the local coordinates, each part in (3.8) is written as  $(dz)_{\parallel} = |dz| = \sqrt{g} \prod_\alpha d\xi^\alpha$  and  $(d\pi)_{\parallel} = (1/\sqrt{g}) \prod_\alpha d\eta_\alpha$  with  $g = \det(g_{\alpha\beta}(\xi))$ .

any motion  $(z, \pi) \xrightarrow{s} (z', \pi')$  obtained by integrating (3.13)–(3.16), its time-reversed motion  $(z', -\pi') \xrightarrow{s} (z, -\pi)$  is also a solution. (3) energy conservation:  $H(z', \pi') = H(z, \pi)$ .

The discrete version of the above molecular dynamics can be given as follows. First we introduce the step size  $\Delta s$  and the following RATTLE process [17, 18] which generates a one-step motion from  $(z, \pi) \in T^*\Sigma$  to  $(z', \pi') \equiv \Phi_{\Delta s}(z, \pi) \in T^*\Sigma$ :

$$\pi_{1/2} = \pi - \frac{\Delta s}{2} \partial V(z) - \frac{\Delta s}{2} \partial \phi^r(z) \lambda_r^{(1)}, \quad (3.17)$$

$$z' = z + \Delta s (M^{-1} \pi_{1/2}), \quad (3.18)$$

$$0 = \phi^r(z'), \quad (3.19)$$

$$\pi' = \pi_{1/2} - \frac{\Delta s}{2} \partial V(z') - \frac{\Delta s}{2} \partial \phi^r(z') \lambda_r^{(2)}, \quad (3.20)$$

$$0 = (M^{-1}\pi') \cdot \partial\phi^r(z'), \quad (3.21)$$

where  $\partial V(z) \equiv (\partial_{z^I} V(z))$ . Note that there appear two Lagrange multipliers.  $\lambda_r^{(1)}$  is determined so that the new configuration  $z'$  is on  $\Sigma$  [ $z' \in \Sigma$ , eq. (3.19)], while  $\lambda_r^{(2)}$  is determined so that  $\pi'$  is in the tangential direction [ $\pi' \in T_{z'}^*\Sigma$ , eq. (3.21)]. One can easily check that  $\Phi_{\Delta s}$  is symplectic ( $d\pi' \wedge dz'|_{T^*\Sigma} = d\pi \wedge dz|_{T^*\Sigma}$ ) and reversible [if  $(z', \pi') = \Phi_{\Delta s}(z, \pi)$  then  $(z, -\pi) = \Phi_{\Delta s}(z', -\pi')$  with the interchange of  $\lambda^{(1)}$  and  $\lambda^{(2)}$ ], and preserves the energy to second order:

$$H(z', \pi') = H(z, \pi) + O(\Delta s^3). \quad (3.22)$$

We need to rewrite the above RATTLE process when, as in Lefschetz thimble methods, we do not know explicit functional forms of the constraint functions  $\phi^r(z)$  except for the bases of the tangent and the normal spaces to  $z$  [ $E_\alpha = (E_\alpha^I)$  and  $F_r = (F_r^I)$ , respectively]. This rewriting can be done in the following way after introducing the orthogonal projector  $\mathcal{P}(z) = (\mathcal{P}^I_J(z))$  from  $T_z^*\mathbb{R}^{2N}$  to  $T_z^*\Sigma$  (see Fig. 1):<sup>14</sup>

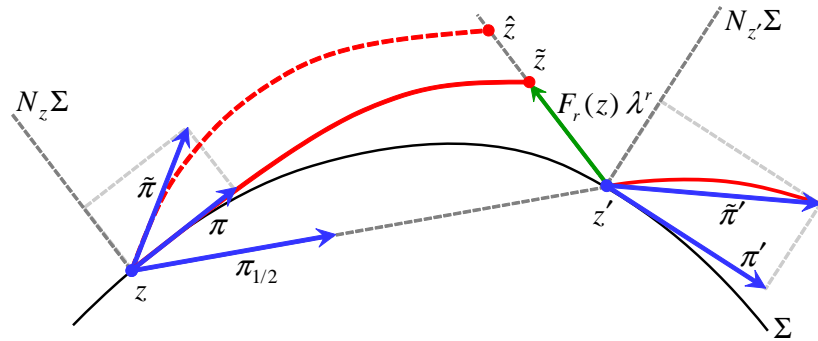


Figure 1: RATTLE process from  $\zeta = (z, \pi) \in T_z^*\Sigma$  to  $\zeta' = (z', \pi') \in T_{z'}^*\Sigma$ .

---

<sup>14</sup>We owe much of the discussions for the RATTLE process on flowed surfaces to [19].

1. For a given  $\zeta = (z, \pi) \in T^*\Sigma$ , we set

$$\tilde{z} \equiv z + \Delta s (M^{-1} \pi) - \frac{\Delta s^2}{2} M^{-1} \partial V(z). \quad (3.23)$$

2. We find  $\lambda^r$  such that

$$z' \equiv \tilde{z} - F_r(z) \lambda^r \in \Sigma. \quad (3.24)$$

3. We define

$$\pi_{1/2} \equiv \frac{1}{\Delta s} M(z' - z), \quad (3.25)$$

and set

$$\tilde{\pi}' \equiv \pi_{1/2} - \frac{\Delta s}{2} \partial V(z'). \quad (3.26)$$

4. We project  $\tilde{\pi}'$  on  $T_{z'}^*\Sigma$ :

$$\pi' \equiv \tilde{\pi}' \mathcal{P}(z'). \quad (3.27)$$

Note that  $\lambda^r$  must be of  $O(\Delta s^2)$ .<sup>15</sup>

### 3.2. Molecular dynamics on a flowed surface $\Sigma_t$

We now apply the formalism developed in the previous subsection to a flowed surface  $\Sigma = \Sigma_t$  in the TLTM, where  $m$  ( $= \dim \Sigma_t$ ) is given by  $N$ .<sup>16</sup> The potential is given by  $V(z) \equiv \text{Re } S(z)$ . A crucial point here is that, although we do not know explicit functional forms of  $\phi^\alpha(z)$ , there is a one-to-one correspondence between points  $z = (z^I) \in \Sigma_t$  and those  $x = (x^\alpha) \in \mathbb{R}^N$  with the relation  $z = z_t(x)$ . Furthermore, the bases of the tangent and normal spaces to  $z = z_t(x)$  can be given explicitly as

$$E_\alpha^I(x) \equiv \partial z_t^I(x) / \partial x^\alpha, \quad F_\alpha^I(x) \equiv (\hat{i} E_\alpha(x))^I \quad (I = 1, \dots, 2N), \quad (3.28)$$

whose complex representations are given by  $E_\alpha^i = \partial z_t^i(x) / \partial x^\alpha$  and  $F_\alpha^i = i E_\alpha^i$  ( $i = 1, \dots, N$ ). Note that  $(E_\alpha^i(x))$  is nothing but the Jacobian matrix  $J(x) = J_R(x) + i J_I(x)$ , whose real

---

<sup>15</sup>Note that the replacement of  $\pi$  in (3.23) by  $\tilde{\pi}$  in Fig. 1 can be totally absorbed by a shift of the Lagrange multiplier  $\lambda^r$ , without changing the location of  $z'$ . With this replacement, we can rewrite the above steps as a procedure to obtain a new pair  $(z', \tilde{\pi}')$  from  $(z, \tilde{\pi})$  as in Fig. 1. The projection (Step 4) is then required only at the final step of molecular dynamics evolution. Note that the Lagrange multiplier will then become of  $O(\Delta s)$ .

<sup>16</sup>We will label the constraints also with  $\alpha$  ( $= 1, \dots, N$ ) instead of  $r$ .

representation is now given by

$$J(x) = (J_A^I(x)) \equiv \begin{pmatrix} (J_R(x))^i{}_\alpha & -(J_I(x))^i{}_\alpha \\ (J_I(x))^i{}_\alpha & (J_R(x))^i{}_\alpha \end{pmatrix} = (E_\alpha(x), F_\alpha(x)) \quad (A = 1, \dots, 2N). \quad (3.29)$$

The (complex-valued) Jacobian matrix  $J(x) = (\partial z_t^i(x)/\partial x^\alpha) \equiv J_t(x)$  obeys the following differential equation in the complex representation [9] (see also footnote 2 of [11]):

$$\dot{J}_t = [H(z_t) \cdot J_t]^*, \quad J_{t=0} = 1_N \quad (3.30)$$

with  $H(z) \equiv (\partial_i \partial_j S(z))$ .

The condition that  $z' \in \Sigma_t \subset \mathbb{R}^{2N}$  for a given  $z = z_t(x)$  [eq. (3.24)] is equivalent to that there be a point  $x' = x + u \in \mathbb{R}^N$  such that  $z'$  can be written as  $z' = z_t(x')$ . Together with the need to find  $\lambda$ , our requirement can be expressed as the following  $2N$  equations for  $2N$  unknown variables  $u^\alpha, \lambda^\alpha$  ( $\alpha = 1, \dots, N$ ):

$$\begin{aligned} 0 &= z_t^I(x + u) - \tilde{z}^I + F_\alpha^I(z) \lambda^\alpha \\ &= z_t^I(x + u) - z_t^I(x) - \Delta s (M^{-1} \pi)^I + \frac{\Delta s^2}{2} (M^{-1} \partial V(z))^I + F_\alpha^I(z) \lambda^\alpha \\ &\equiv f^I(u, \lambda; x). \end{aligned} \quad (3.31)$$

This equation can be solved iteratively for

$$w = (w^A) = \begin{pmatrix} u^\alpha \\ \lambda^\alpha \end{pmatrix} \quad (3.32)$$

with Newton's method. Namely, starting from an initial guess  $w_0 = (w_0^A)$ , we obtain a sequence  $w_k \rightarrow w_{k+1} = w_k + \Delta w$  by solving the linear equation

$$\frac{\partial f^I}{\partial w^A} \Big|_{w_k} \Delta w^A = -f^I(w_k). \quad (3.33)$$

Here, from the explicit form of  $f^I$ , we find that

$$\frac{\partial f^I}{\partial u^\alpha} = \frac{\partial z^I(x + u)}{\partial u^\alpha} = \frac{\partial z^I(x)}{\partial x^\alpha} \Big|_{x+u} = E_\alpha^I(x + u), \quad (3.34)$$

$$\frac{\partial f^I}{\partial \lambda^\alpha} = F_\alpha^I(x), \quad (3.35)$$

and thus the recursive equation can be written as

$$(E_\alpha(x + u_k), F_\alpha(x)) \begin{pmatrix} \Delta u^\alpha \\ \Delta \lambda^\alpha \end{pmatrix} = -f(w_k), \quad (3.36)$$

or equivalently,

$$\begin{pmatrix} J_R(x + u_k) & -J_I(x) \\ J_I(x + u_k) & J_R(x) \end{pmatrix} \begin{pmatrix} \Delta u \\ \Delta \lambda \end{pmatrix} = -f(w_k). \quad (3.37)$$

The linear equation (3.37) can be solved in two ways. One is to directly obtain all the matrix elements of the Jacobian matrices  $J(x) = J_R(x) + i J_I(x)$  and  $J(x + u_k) = J_R(x + u_k) + i J_I(x + u_k)$  by numerically integrating (2.9) and (3.30) and then to obtain the solution  $\Delta w = (\Delta u, \Delta \lambda)^T$  with a direct method such as the LU decomposition. The other method is to use an iterative method such as GMRES [27] or BiCGStab [28] without calculating the matrix elements explicitly (as in [29]). The reason why such a method is possible here is that the left-hand side of (3.37) can be rewritten as

$$\begin{pmatrix} J_R(x + u_k) & -J_I(x + u_k) \\ J_I(x + u_k) & J_R(x + u_k) \end{pmatrix} \begin{pmatrix} \Delta u \\ 0 \end{pmatrix} + \hat{i} \begin{pmatrix} J_R(x) & -J_I(x) \\ J_I(x) & J_R(x) \end{pmatrix} \begin{pmatrix} \Delta \lambda \\ 0 \end{pmatrix}, \quad (3.38)$$

and each term can be evaluated by numerically integrating the following differential equations for  $z_t = (z_t^I)$  and a vector  $v_t = (v_t^I)$  (not for a matrix):

$$\dot{z}_t = \hat{C} \partial \operatorname{Re} S(z_t), \quad (3.39)$$

$$\dot{v}_t = \hat{C} H(z_t) v_t = \begin{pmatrix} H_R(z_t) & -H_I(z_t) \\ -H_I(z_t) & -H_R(z_t) \end{pmatrix} v_t \quad (3.40)$$

with the initial conditions  $z_0 = x + u_k$  and  $v_0 = (\Delta u, 0)^T$  or  $z_0 = x$  and  $v_0 = (\Delta \lambda, 0)^T$ .<sup>17</sup>

In the above procedure, one needs to use the projector  $\mathcal{P}(z) = (\mathcal{P}^I J(z))$  that projects  $\tilde{\pi} \in T_z^* \mathbb{R}^{2N}$  to  $\pi = \tilde{\pi} \mathcal{P}(z) \in T_z^* \Sigma_t$  at  $z = z_t(x)$ , or equivalently, that projects  $\tilde{v} \equiv M^{-1} \tilde{\pi} \in T_z \mathbb{R}^{2N}$  to  $v \equiv M^{-1} \pi = \mathcal{P}(z) \tilde{v} \in T_z \Sigma_t$  at  $z = z_t(x)$ . The projection can also be given in two ways. When the matrix elements of  $J(x)$  are known explicitly as in the direct method given in the previous paragraph, the matrix  $\mathcal{P} = (\mathcal{P}^I J = E_\alpha^I E_J^\alpha)$  can also be calculated explicitly as

$$\mathcal{P} = (E_\alpha^I) (E_J^\alpha) = (E_\alpha^I, F_\alpha^I) \begin{pmatrix} \delta_\beta^\alpha & 0 \\ 0 & 0 \end{pmatrix} \begin{pmatrix} E_J^\beta \\ F_J^\beta \end{pmatrix} = J(x) \widehat{\operatorname{Re}} J^{-1}(x), \quad (3.41)$$

whose complex representation is given by  $v = J(x) \operatorname{Re}[J^{-1}(x) \tilde{v}]$  for complex vectors  $v = (v^i)$ ,  $\tilde{v} = (\tilde{v}^i) \in \mathbb{C}^N$ .<sup>18</sup> The other method does not require an explicit knowledge of the

---

<sup>17</sup>The complex representation of (3.39) and (3.40) for  $z_t = (z_t^i)$ ,  $v_t = (v_t^i) \in \mathbb{C}^N$  are given, respectively, by

$$\dot{z}_t^i = [\partial_i S(z_t)]^*, \quad \dot{v}_t^i = [H_{ij}(z_t) v_t^j]^*.$$

The initial conditions are given by  $z_0^i = x^i + u_k^i$  and  $v_0^i = \Delta u^i$  or  $z_0^i = x^i$  and  $v_0^i = \Delta \lambda^i$  for  $\Delta u, \Delta \lambda \in \mathbb{R}^N$ .

<sup>18</sup>This expression first appeared in [7] as the projection on the tangent space to a critical point of a Lefschetz thimble.

matrix elements of  $J(x)$  (as in [29]). We here demonstrate this procedure in the complex representation. We first find two real column vectors  $a, b \in \mathbb{R}^N$  such that they satisfy a linear equation

$$J(x) a + i J(x) b = \tilde{v} \in \mathbb{C}^N. \quad (3.42)$$

Here,  $J(x) a$  and  $J(x) b$  are obtained by numerically integrating (3.39) and (3.40) with the initial conditions  $(z_0, v_0) = (x, a)$  and  $(z_0, v_0) = (x, b)$ , respectively. The linear equation (3.42) can be solved for  $a, b$  with an iterative method. Once  $a$  and  $b$  are obtained,  $v$  is given by  $J(x) a$  (which we already have in the above process) because the formal solution for  $a$  is given by  $a = \text{Re}[J^{-1}(x) \tilde{v}]$ .

We summarize the algorithm for a molecular dynamics on  $T^*\Sigma_t$  that updates a configuration from  $\zeta = (z, \pi) \in T^*\Sigma_t$  with  $z = z_t(x)$  to  $\zeta' = (z', \pi') = \Phi_{\Delta s}(z, \pi) \in T^*\Sigma_t$  with  $z' = z_t(x')$ . Every step below will be mostly given in the real representation, which can be readily translated to the complex representation.

**Step 1.** For  $\zeta = (z, \pi) \in T^*\Sigma_t$  with  $z = z_t(x)$ , we find  $w = (u, \lambda)^T = ((u^\alpha), (\lambda^\alpha))^T$  ( $\alpha = 1, \dots, N$ ) that satisfies (3.31). The equation can be solved iteratively,  $w_k \rightarrow w_{k+1} = w_k + \Delta w$ , with Newton's method, starting from an initial guess  $w_0 = (u_0, \lambda_0)^T$  and solving the linear equation (3.37) to obtain  $\Delta w = (\Delta u, \Delta \lambda)^T$ . Equation (3.37) can be solved with either of a direct method or an iterative method. After  $w = (u, \lambda)^T$  is obtained, we set  $x' = x + u$  and  $z' = z_t(x')$ .

**Step 2.** Define

$$\pi_{1/2} \equiv \frac{1}{\Delta s} M(z' - z), \quad (3.43)$$

and set

$$\tilde{\pi}' \equiv \pi_{1/2} - \frac{\Delta s}{2} \partial V(z'). \quad (3.44)$$

**Step 3.** Project  $\tilde{v}' \equiv M^{-1} \tilde{\pi}'$  to  $v' = \mathcal{P}(z') \tilde{v}' \in T_{z'} \Sigma_t$  to obtain  $\pi' = M v' \in T_{z'}^* \Sigma_t$ . The projection can be made with a direct method when the matrix elements of  $J(x')$  are known explicitly, or with an iterative method.

In practice, since  $\Delta s$  is finite, it can happen, for  $z$  close to zeros of the weight  $e^{-S(z)}$ , that one cannot find a solution  $z' = z_t(x')$  to (3.33) anywhere in  $\mathbb{C}^N$  or can only find a solution beyond the zeros. When this happens, we replace  $\Phi_{\Delta s}$  by a *momentum flip*  $\Psi$  that is defined by<sup>19</sup>

$$\Psi(z, \pi) = (z, -\pi). \quad (3.45)$$

---

<sup>19</sup>Note that such an aggressive withdrawal is allowed as an algorithm because a detour to go around zeros are provided by the tempering.

Note that  $\Psi$  is also volume-preserving and reversible [if  $\Psi(z, \pi) = (z', \pi')$  then  $\Psi(z', -\pi') = (z, -\pi)$ ]. To understand the reversibility, consider a move of a molecule in the forward and backward directions in  $s$ , each consisting of three steps (see Fig. 2):

$$\text{forward: } (z_0, \pi_0) \xrightarrow{\Phi_{\Delta s}} (z_1, \pi_1) \xrightarrow{\Psi} (z_2, \pi_2) \xrightarrow{\Phi_{\Delta s}} (z_3, \pi_3), \quad (3.46)$$

$$\text{backward: } (\tilde{z}_0, \tilde{\pi}_0) \xrightarrow{\Phi_{\Delta s}} (\tilde{z}_1, \tilde{\pi}_1) \xrightarrow{\Psi} (\tilde{z}_2, \tilde{\pi}_2) \xrightarrow{\Phi_{\Delta s}} (\tilde{z}_3, \tilde{\pi}_3) \quad (3.47)$$

with  $(\tilde{z}_0, \tilde{\pi}_0) \equiv (z_3, -\pi_3)$ . There, we assume that a move from  $z_1$  with  $\pi_1$  is prohibited by a

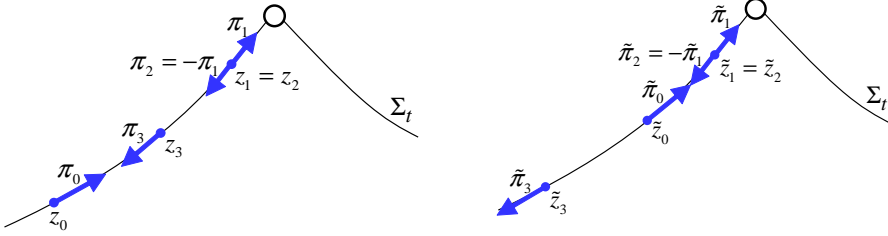


Figure 2: Moves on  $\Sigma_t$  near a zero of  $e^{-S(z)}$  (indicated by a circle). (Left) An original forward move with a momentum flip at  $z_1$ . (Right) The time-reversed backward move.

prescribed condition. We thus flip the momentum from  $\pi_1$  to  $\pi_2 = -\pi_1$ , and the molecule arrives at  $z_3$  with  $\pi_3$ . As for the backward move starting from  $\tilde{z}_0 = z_3$  with  $\tilde{\pi}_0 = -\pi_3$ , it will arrive at  $\tilde{z}_1 = z_2$  with  $\tilde{\pi}_1 = -\pi_1$  thanks to the reversibility of  $\Phi_{\Delta s}$ . Then the further move with  $\tilde{\pi}_1$  must be prohibited by the same condition that prohibited the further move from  $z_1$  with  $\pi_1$ . Then we make a momentum flip from  $\tilde{\pi}_1$  to  $\tilde{\pi}_2 = -\tilde{\pi}_1$ , and the molecule will arrive at  $\tilde{z}_3$  which must coincide with  $z_0$  again thanks to the reversibility of  $\Phi_{\Delta s}$ . We thus see that the reversibility holds for the whole process with the relation  $(\tilde{z}_n, \tilde{\pi}_n) = (z_{3-n}, -\pi_{3-n})$ .

Due to the volume-preservation and the reversibility of  $\Phi_{\Delta s}$  and  $\Psi$ , the transition probability

$$\mathbb{P}^{(1)}(\zeta'|\zeta) \equiv \min\left(1, e^{-H(\zeta')+H(\zeta)}\right) \delta(\zeta' - \Phi_{\Delta s}^n(\zeta)) \quad (\zeta' \neq \zeta) \quad (3.48)$$

satisfies the following relation [see (2.16) and (2.17)]:

$$\mathbb{P}^{(1)}(\zeta'|\zeta) e^{-H(\zeta)} = \mathbb{P}^{(1)}(\zeta^T|\zeta'^T) e^{-H(\zeta')} \quad (3.49)$$

even when the partial replacements from  $\Phi_{\Delta s}$  to  $\Psi$  are made. In the following, we only use the symbol  $\Phi_{\Delta s}$  with the understanding that it will be replaced by  $\Psi$  when necessary.

## 4. HMC on TLTM

In this section, after introducing a method to swap configurations at adjacent replicas, we summarize the HMC algorithm on TLTM.

## 4.1. Swap of configurations at adjacent replicas

We realize the swap of configurations at adjacent replicas,  $\Sigma_{t_a}$  and  $\Sigma_{t_b}$  ( $b = a \pm 1$ ), by the *exchange of the initial configurations*. Namely,  $(z_a, z_b) \equiv (z_{t_a}(x), z_{t_b}(y)) \in \Sigma_{t_a} \times \Sigma_{t_b}$  is proposed to be updated to  $(z'_a, z'_b) \equiv (z_{t_a}(x'), z_{t_b}(y')) \in \Sigma_{t_a} \times \Sigma_{t_b}$  with  $(x', y') = (y, x)$  (see Fig. 3). Accordingly, the accept/reject probability must be with respect to  $x = (x^i) \in \mathbb{R}^N$ ,

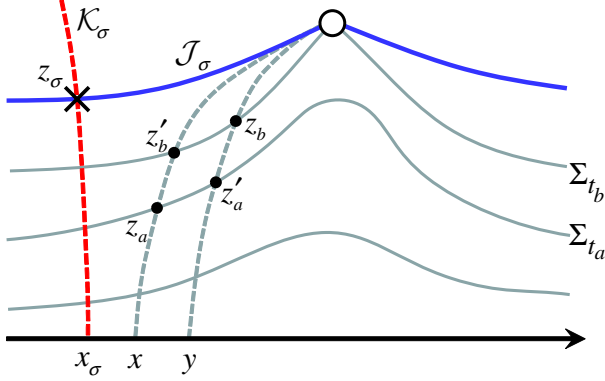


Figure 3: Swap of configurations from  $(z_a, z_b) \equiv (z_{t_a}(x), z_{t_b}(y)) \in \Sigma_{t_a} \times \Sigma_{t_b}$  to  $(z'_a, z'_b) \equiv (z_{t_a}(y), z_{t_b}(x)) \in \Sigma_{t_a} \times \Sigma_{t_b}$ , which is actually the exchange of the initial configurations  $x$  and  $y$ . In figure,  $\mathcal{J}_\sigma$  is the Lefschetz thimble associated to a critical point  $z_\sigma$ .  $\mathcal{K}_\sigma$  is the corresponding anti-thimble. The distribution  $\propto e^{-\text{Re } S(z)}$  on  $\Sigma_t$  has peaks at intersection points  $x_\sigma$  of  $\Sigma_t$  and  $\mathcal{K}_\sigma$ .

and the algorithm takes the following form:

1. We first calculate the Jacobian matrices  $J_a \equiv J_{t_a}(x)$ ,  $J_b \equiv J_{t_b}(y)$ .
2. We further calculate  $z'_a \equiv z_{t_a}(y)$  and  $z'_b \equiv z_{t_b}(x)$  together with the corresponding Jacobian matrices,  $J'_a \equiv J_{t_a}(y)$  and  $J'_b \equiv J_{t_b}(x)$ .
3. We update the original initial configurations  $(x, y)$  to the swapped initial configurations  $(x', y') = (y, x)$  with the probability

$$\min \left( 1, \frac{|\det J'_a| |\det J'_b| e^{-V(z'_a) - V(z'_b)}}{|\det J_a| |\det J_b| e^{-V(z_a) - V(z_b)}} \right). \quad (4.1)$$

The above procedure correctly leads to the global equilibrium on the product space  $\Sigma_{\text{tot}} = \Sigma_{t_0} \times \dots \times \Sigma_{t_A}$  with the distribution  $p_{\text{eq}}(\vec{z}) \prod_{a=0}^A |dz_a| \propto \prod_{a=0}^A e^{-V(z_a)} |dz_a|$ . In fact, by using  $|dz| = |\det J(x)| dx$ , the transition probability  $\hat{P}_{ab}^{(2)}(x', y' | x, y)$  from  $(x, y) \in \mathbb{R}^N \times \mathbb{R}^N$  to  $(x', y') \in \mathbb{R}^N \times \mathbb{R}^N$  can be rewritten to the transition probability  $P_{ab}^{(2)}(z'_a, z'_b | z_a, z_b)$  from  $(z_a, z_b) = (z_{t_a}(x), z_{t_b}(y)) \in \Sigma_{t_a} \times \Sigma_{t_b}$  to  $(z'_a, z'_b) = (z_{t_a}(x'), z_{t_b}(y')) \in \Sigma_{t_a} \times \Sigma_{t_b}$  as follows:

$$P_{ab}^{(2)}(z'_a, z'_b | z_a, z_b) = |\det J_{t_a}(x')|^{-1} |\det J_{t_b}(y')|^{-1} \hat{P}_{ab}^{(2)}(x', y' | x, y), \quad (4.2)$$

which means that the transition probability for  $(x, y) \rightarrow (x', y')$  is translated to the following probability for  $(z_a, z_b) \rightarrow (z'_a, z'_b)$ :

$$P_{ab}^{(2)}(z'_a, z'_b | z_a, z_b) = \min \left( \frac{1}{|\det J'_a| |\det J'_b|}, \frac{e^{-V(z'_a) - V(z'_b)}}{|\det J_a| |\det J_b| e^{-V(z_a) - V(z_b)}} \right) \times \delta(x' - y) \delta(y' - x) \quad [(z'_a, z'_b) \neq (z_a, z_b)]. \quad (4.3)$$

Then one can easily show that the following detailed balance condition does hold:

$$P_{ab}^{(2)}(z'_a, z'_b | z_a, z_b) e^{-V(z_a) - V(z_b)} = P_{ab}^{(2)}(z_a, z_b | z'_a, z'_b) e^{-V(z'_a) - V(z'_b)}. \quad (4.4)$$

Note that we have to calculate the Jacobian determinant explicitly at every swapping process even though this is not mandatory for the molecular dynamics on each flowed surface.

We make an important comment on the reason why we use initial configurations as a reference in the swapping process. In general, one can introduce an arbitrary (global) coordinate system to each flowed surface, to be used as a reference in swapping configurations as above. However, for such arbitrarily chosen coordinate systems, the distributions as functions of the coordinates will take very different functional forms between adjacent replicas, and one cannot expect a significant acceptance rate. On the other hand, this problem will not occur if we take the initial configurations as a common reference, because the distributions then have peaks at the same coordinate values (such as  $x_\sigma$  in Fig. 3 that flows to a critical point  $z_\sigma$ ) for different flowed surfaces [12].

Another comment is that one can extend the molecular dynamics to the phase space of the whole enlarged configuration space,  $T^*\Sigma_{t_0} \times \dots \times T^*\Sigma_{t_A}$ , also by swapping momenta  $\pi_a$  in the course of molecular dynamics, as in [30]. However, the additional computational cost will not be negligible, because in TLTM we need to transport  $\pi_a \in T^*\Sigma_{t_a}$  (*resp.*  $\pi_b \in T^*\Sigma_{t_b}$ ) to obtain  $\pi'_b \in T^*\Sigma_{t_b}$  (*resp.*  $\pi'_a \in T^*\Sigma_{t_a}$ ), and such a transport generically causes an additional difference in the sum of Hamiltonians, which lowers acceptance rates. We leave the investigation of this algorithm and the study of its effectiveness for future work.

## 4.2. Summary of HMC on TLTM

We summarize the HMC algorithm on the TLTM by following the outline given in subsection 2.3 (recall that  $V(z) = \text{Re } S(z)$ ):

**Step A. HMC on  $\{\Sigma_{t_a}\}$ :**

**Step A1. Initial setup:**

For a given configuration  $\vec{z} = (z_a = z_{t_a}(x_a)) \in \Sigma_{\text{tot}} = \Sigma_{t_0} \times \dots \times \Sigma_{t_A}$ , we generate  $\tilde{\vec{\pi}} = (\tilde{\pi}_a) \in \mathbb{R}^{2N} \times \dots \times \mathbb{R}^{2N}$  with a Gaussian distribution  $\propto \prod_a e^{-\tilde{\pi}_a^2/2M_a}$ , and

project it on  $T_{z_0}^* \Sigma_{t_0} \times \cdots \times T_{z_A}^* \Sigma_{t_A}$  to obtain  $\pi_a = \tilde{\pi}_a \mathcal{P}(z_a)$ . The projection can be made with a direct method when the matrix elements of  $J_a \equiv J_{t_a}(x_a)$  are known explicitly, or with an iterative method.

**Step A2.** For each  $\zeta_a = (z_a, \pi_a) \in T^* \Sigma_{t_a}$  with  $z_a = z_{t_a}(x_a)$ , we find  $w = (u, \lambda)^T$  that satisfies (3.31). The equation can be solved iteratively,  $w_k \rightarrow w_{k+1} = w_k + \Delta w$ , with Newton's method, starting from an initial guess  $w_0 = (u_0, \lambda_0)^T$  and solving the linear equation (3.37) to obtain  $\Delta w = (\Delta u, \Delta \lambda)^T$ . Equation (3.37) can be solved with either of a direct method or an iterative method. After  $w = (u, \lambda)^T$  is obtained, we set  $x'_a = x_a + u$  and  $z'_a = z_{t_a}(x'_a)$ .

**Step A3.** For each replica  $a$ , we define

$$\pi_{a,1/2} \equiv \frac{1}{\Delta s} M(z'_a - z_a), \quad (4.5)$$

and set

$$\tilde{\pi}'_a \equiv \pi_{a,1/2} - \frac{\Delta s}{2} \partial \text{Re} S(z'_a). \quad (4.6)$$

**Step A4.** For each replica  $a$ , we project  $\tilde{\pi}'_a$  on  $T_{z'_a}^* \Sigma_{t_a}$  to obtain  $\pi'_a = \tilde{\pi}'_a \mathcal{P}(z')$ . The projection can be made with a direct method when the matrix elements of  $J'_a$  are known explicitly, or with an iterative method.

**Step A5.** We repeat Steps A2 through A4 a fixed number of times ( $\equiv n$ ) for all replicas.

**Step A6.** We calculate  $\Delta H_a \equiv H_a(\zeta'_a) - H_a(\zeta_a)$ , and update  $\zeta_a$  to  $\zeta'_a$  with the probability  $\min(1, e^{-\Delta H_a})$ .

**Step A7.** We ignore the values of  $\pi'_a$  and only consider those of  $z'_a$ .

**Step B. Swap among  $\{\Sigma_{t_a}\}$ :**

**Step B1.** For a given pair  $(z_a, z_b) = (z_{t_a}(x), z_{t_b}(y)) \in \Sigma_{t_a} \times \Sigma_{t_b}$ , we calculate the Jacobian matrices  $J_a \equiv J_{t_a}(x)$ ,  $J_b \equiv J_{t_b}(y)$  if they have not been calculated yet.

**Step B2.** We calculate  $z'_a \equiv z_{t_a}(y)$  and  $z'_b \equiv z_{t_b}(x)$  together with the corresponding Jacobian matrices,  $J'_a \equiv J_{t_a}(y)$  and  $J'_b \equiv J_{t_b}(x)$ , by numerically integrating the flow equations (2.9) and (3.30).

**Step B3.** We update the original initial configurations  $(x, y)$  to the swapped initial configurations  $(x', y') = (y, x)$  with the probability

$$\min \left( 1, \frac{|\det J'_a| |\det J'_b| e^{-\text{Re} S(z'_a) - \text{Re} S(z'_b)}}{|\det J_a| |\det J_b| e^{-\text{Re} S(z_a) - \text{Re} S(z_b)}} \right). \quad (4.7)$$

**Step C.** After repeating Steps A and B sufficiently many times, we make a measurement and save the values  $\{e^{i\theta(z_a)}, \mathcal{O}(z_a)\}$  ( $a = 0, \dots, A$ ), that are calculated from  $z_a$  and  $J_a$ .

## 5. Results and analysis

In this section, we apply the TLTM to the Hubbard model both with HMC (implemented in this paper) and with Metropolis (adopted in [11, 12]). We first confirm both algorithms to work correctly by showing that they correctly estimate the expectation value of the number density operator. We then show that HMC is more efficient than Metropolis even for small degrees of freedom ( $N = 20$ ).

### 5.1. Hubbard model and the parameters for simulations

The Hubbard model is defined by the Hamiltonian

$$H = -\kappa \sum_{\mathbf{x}, \mathbf{y}} \sum_{\sigma} K_{\mathbf{xy}} c_{\mathbf{x}, \sigma}^{\dagger} c_{\mathbf{y}, \sigma} - \mu \sum_{\mathbf{x}} (n_{\mathbf{x}, \uparrow} + n_{\mathbf{x}, \downarrow} - 1) + U \sum_{\mathbf{x}} (n_{\mathbf{x}, \uparrow} - 1/2) (n_{\mathbf{x}, \downarrow} - 1/2). \quad (5.1)$$

Here,  $c_{\mathbf{x}, \sigma}$  and  $c_{\mathbf{x}, \sigma}^{\dagger}$  are the annihilation and creation operators on site  $\mathbf{x} \in \Lambda$  with spin  $\sigma$  ( $= \uparrow, \downarrow$ ), obeying  $\{c_{\mathbf{x}, \sigma}, c_{\mathbf{y}, \tau}^{\dagger}\} = \delta_{\mathbf{xy}} \delta_{\sigma \tau}$  and  $\{c_{\mathbf{x}, \sigma}, c_{\mathbf{y}, \tau}\} = \{c_{\mathbf{x}, \sigma}^{\dagger}, c_{\mathbf{y}, \tau}^{\dagger}\} = 0$ , and  $n_{\mathbf{x}, \sigma} \equiv c_{\mathbf{x}, \sigma}^{\dagger} c_{\mathbf{x}, \sigma}$ .  $K_{\mathbf{xy}}$  is the adjacency matrix that takes a nonvanishing value ( $\equiv 1$ ) only for nearest neighbors, and we assume the lattice to be bipartite.  $\kappa$  ( $> 0$ ) is the hopping parameter,  $\mu$  is the chemical potential, and  $U$  ( $> 0$ ) represents the strength of the on-site repulsive potential.  $n_{\mathbf{x}, \sigma}$  is shifted as  $n_{\mathbf{x}, \sigma} - 1/2$  such that  $\mu = 0$  corresponds to the half-filling state,  $\sum_{\sigma} \langle n_{\mathbf{x}, \sigma} - 1/2 \rangle = 0$ .

By using the Trotter decomposition with equal spacing  $\epsilon$  ( $\beta = N_{\tau} \epsilon$ ), we can rewrite the expectation value of the number density  $n \equiv (1/N_s) \sum_{\mathbf{x}} (n_{\mathbf{x}, \uparrow} + n_{\mathbf{x}, \downarrow} - 1)$  as a path integral over a Gaussian Hubbard-Stratonovich variable  $\phi = (\phi_{\ell, \mathbf{x}})$  as follows (see, e.g., [12] for the derivation):

$$\langle n \rangle \equiv \frac{\int d\phi e^{-S(\phi)} n(\phi)}{\int d\phi e^{-S(\phi)}} \quad \left( d\phi \equiv \prod_{\ell, \mathbf{x}} d\phi_{\ell, \mathbf{x}} \right), \quad (5.2)$$

$$e^{-S(\phi)} \equiv e^{-(1/2) \sum_{\ell, \mathbf{x}} \phi_{\ell, \mathbf{x}}^2} \det M^a(\phi) \det M^b(\phi), \quad (5.3)$$

$$M^{a/b}(\phi) \equiv 1 + e^{\pm \beta \mu} \prod_{\ell} e^{\epsilon \kappa K} e^{\pm i \sqrt{\epsilon U} \phi_{\ell}}, \quad (5.4)$$

$$n(\phi) \equiv (i \sqrt{\epsilon U} N_{\tau} N_s)^{-1} \sum_{\ell, \mathbf{x}} \phi_{\ell, \mathbf{x}}, \quad (5.5)$$

where  $\phi_{\ell} \equiv (\phi_{\ell, \mathbf{x}} \delta_{\mathbf{xy}})$  and  $\prod_{\ell}$  is a product in descending order. Below we apply the TLTM to this model, in which the variables  $\phi = (\phi_{\ell, \mathbf{x}})$  correspond to  $x = (x^i)$  with  $i = 1, \dots, N$  ( $\equiv N_{\tau} N_s$ ).

We use a two-dimensional periodic square lattice of size  $2 \times 2$  (thus  $N_s = 4$ ). The parameters in the Hamiltonian are set to  $\beta \kappa = 3$ ,  $\beta \mu = 4$ ,  $\beta U = 13$ . The imaginary time

is decomposed to  $N_\tau = 5$  pieces. We set  $A = 6$ ,  $T = 0.24$  (maximum flow time), and  $t_a$ 's are set linearly in  $a$ .<sup>20</sup> We use as an initial configuration the one obtained after test runs. The same initial configuration is used for HMC and Metropolis. After discarding 2,000 configurations to ensure equilibration, we take  $N_{\text{conf}} = 30,000$  configurations for estimations. In both algorithms, we first perform swapping process, then make transitions on each flowed surface, and finally make measurements.

In molecular dynamics, we set the step size to  $\Delta s = 0.1$  and the step number to  $n = 10$ . We set  $\sigma_a^2 = 1$  in  $M_{a,II} = \sigma_a^2 \delta_{II}$  for all  $a$ , and use the direct methods for the inversions in Steps A1, A2 and A4 in subsection 4.2. In solving (3.33) iteratively, we set the initial guess to  $w_0 = 0$ , and rescale  $\Delta w$  as  $\Delta w \rightarrow 0.15 \times \Delta w$  when  $|\Delta w|/\sqrt{2N}$  happens to be larger than  $0.5 \times \Delta s / |\det J_{t_a}(x)|^{1/N}$  or when  $|f(w_k + \Delta w)| > |f(w_k)|$ . These prescriptions are to make the updates as local as possible. The stopping criterion is set to  $|\Delta w| < 10^{-8}$  and  $|f(w_k)| < 10^{-5}$ . We find that the iteration process ends up with 3–7 times in most cases. The momentum is flipped either when the number of iterations exceeds 50 or when  $x + u_k + \Delta u$  still flows to a zero of  $e^{-S(z)}$  even after the rescaling  $\Delta w \rightarrow 0.15^3 \times \Delta w$ . The reversibility is tested for some chosen configurations in the vicinity of zeros of  $e^{-S(z)}$ , and it turns out that  $|z' - z|/\sqrt{2N}$  is around  $O(10^{-10})$  for  $(z', \pi') = (\Phi_{\Delta s}^{n=10} \circ \Psi \circ \Phi_{\Delta s}^{10})(z, \pi)$  where  $\pi$  is generated from a Gaussian distribution with unit variance.

For Metropolis, we use the isotropic Gaussian proposals of the standard deviations  $\sigma_{\text{Met}} = 0.037 - 0.18$  (varying on replicas), which are tuned so that the acceptance rate is 0.5–0.7 (see Table 1). We repeat these procedures  $n_{\text{Met}} = 50$  times before moving to the swapping process.

The swapping process is performed by pairing seven replicas in two different ways. One is (i):  $(a, b) = (0, 1), (2, 3), (4, 5)$  leaving replica 6 intact, and the other is (ii):  $(1, 2), (3, 4), (5, 6)$  leaving replica 0 intact. We repeat the swaps seven times changing the pairing (i) and (ii) alternately.<sup>21</sup> The acceptance rates thus obtained are shown in Table 2.<sup>22</sup>

algorithm	parameter	$a = 0$	1	2	3	4	5	6
HMC	$\Delta s$	0.1	0.1	0.1	0.1	0.1	0.1	0.1
	$n$	10	10	10	10	10	10	10
Metropolis	$\sigma_{\text{Met}}$	0.18	0.13	0.10	0.081	0.066	0.038	0.037
	$n_{\text{Met}}$	50	50	50	50	50	50	50

Table 1: The parameters in HMC and Metropolis.

<sup>20</sup>See [12] for a justification of the linear spacing that is based on the geometrical optimization [31, 32].

<sup>21</sup>By making such pairs of independent replicas, swaps can be performed in parallel processes.

<sup>22</sup>The acceptance rates for HMC may seem too large and can actually be reduced by increasing  $\Delta s$ . Note that this must be done carefully, because for too large  $\Delta s$  Newton's method in solving (3.33) may converge to unwanted solutions, which violates the reversibility.

algorithm	direction	$a = 0$	1	2	3	4	5	6
HMC (w/ swap)	$x$ (or $z$ )	0.99	0.98	0.96	0.95	0.94	0.94	0.94
	$a$	0.52	0.48	0.47	0.46	0.46	0.45	-
Metropolis (w/ swap)	$x$ (or $z$ )	0.53	0.54	0.55	0.55	0.55	0.66	0.61
	$a$	0.52	0.48	0.47	0.46	0.46	0.45	-
HMC (w/o swap)	$x$ (or $z$ )	0.99	0.98	0.96	0.95	0.94	0.91	0.96
Metropolis (w/o swap)	$x$ (or $z$ )	0.53	0.54	0.55	0.55	0.55	0.57	0.67

Table 2: The average acceptance rates.

Calculations without swap are also carried out for comparison, with the same parameters and the same initial configuration as those for the calculations with swap.

## 5.2. Estimate of the number density

In order to confirm the algorithms to work correctly, we evaluate the expectation values of the number density  $\langle n \rangle$ . The sign averages and the expectation values are shown in Figs. 4 and 5. We fit the data points in the range  $a = 3, \dots, 6$  for both algorithms, which are

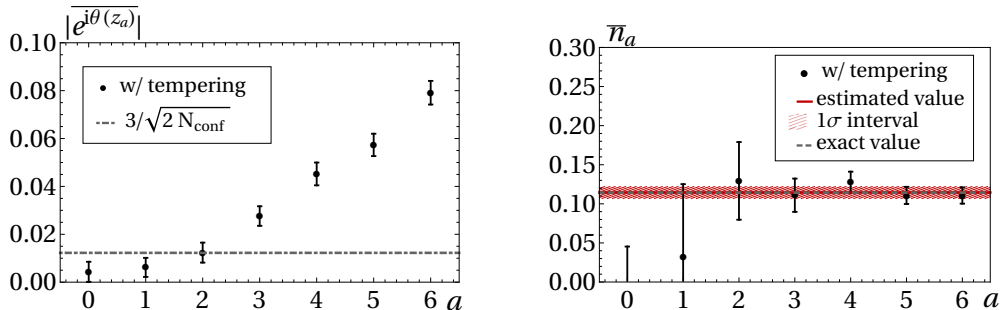


Figure 4: The results for HMC with swap. (Left) The sign averages. (Right) The estimates  $\bar{n}_a$ .

chosen by observing that  $|e^{i\theta(z_a)}|$  are above  $3/\sqrt{2N_{\text{conf}}}$  including the error margin [12]. The results are  $\langle n \rangle \approx 0.1145 \pm 0.0076$  for HMC ( $\chi^2/\text{DOF} = 0.48$ ), and  $\langle n \rangle \approx 0.120 \pm 0.011$  for Metropolis ( $\chi^2/\text{DOF} = 0.44$ ), that should be compared with the exact value  $\langle n \rangle = 0.1143$  (the value under the Trotter decomposition), and thus we confirm that the algorithms work correctly.

We also plot the sign averages and the expectation values obtained without swap in Figs. 6 and 7. For large  $t$ , we observe significant deviations from the exact value but small error margins, reflecting the presence of the ergodicity problem [12].

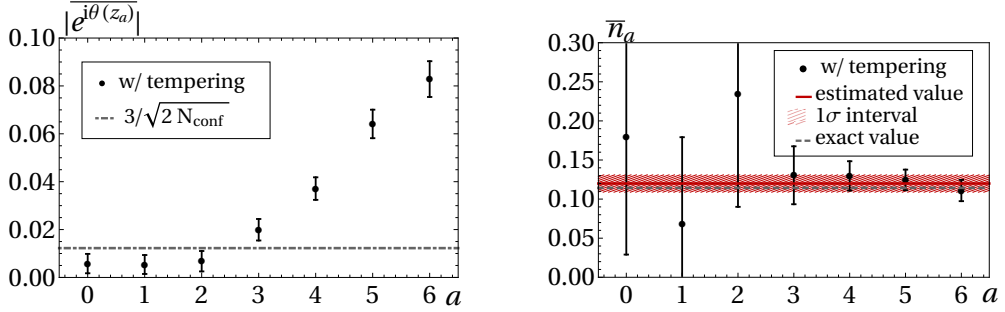


Figure 5: The results for Metropolis with swap. (Left) The sign averages. (Right) The estimates  $\bar{n}_a$ .

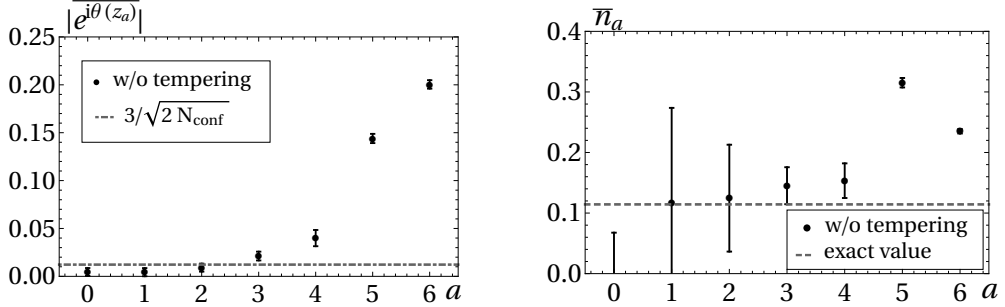


Figure 6: The results for HMC without swap. (Left) The sign averages. (Right) The estimates  $\bar{n}_a$ .

### 5.3. Autocorrelations

In this subsection, we evaluate the autocorrelations for both HMC and Metropolis, and compare their efficiencies. For the evaluation, we estimate the normalized autocorrelation function by (see, e.g., [33, 34])

$$\rho(m) = \frac{C(m)}{C(0)}. \quad (5.6)$$

Here,  $C(m)$  is given by

$$C(m) \equiv \frac{1}{N_{\text{conf}} - m} \sum_{k=1}^{N_{\text{conf}}-m} [f(z_a^{(k)}) - \bar{f}(z_a)][f(z_a^{(k+m)}) - \bar{f}(z_a)], \quad (5.7)$$

where  $\bar{f}(z_a)$  is a sample average for the subsample at replica  $a$ ,  $\bar{f}(z_a) \equiv (1/N_{\text{conf}}) \sum_{k=1}^{N_{\text{conf}}} f(z_a^{(k)})$  (see subsection 2.1). Then, we estimate the integrated autocorrelation time by the following formula, which is valid for  $\tau_{\text{int}} \ll k_{\text{max}} \ll N_{\text{conf}}$  [34]:

$$\tau_{\text{int}} = 1 + 2 \sum_{k=1}^{k_{\text{max}}} \rho(k). \quad (5.8)$$

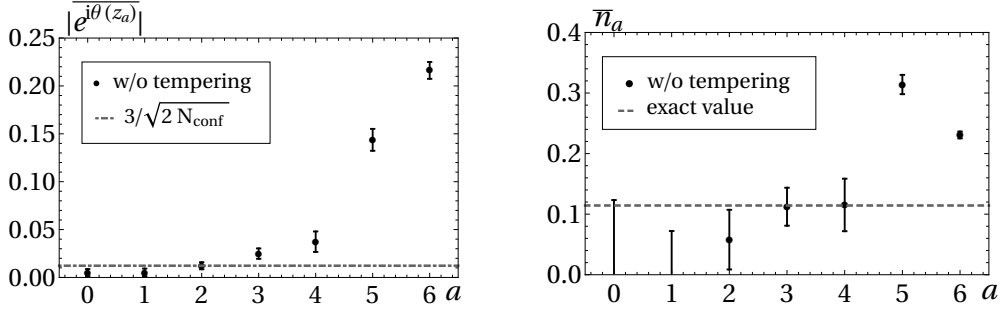


Figure 7: The results for Metropolis without swap. (Left) The sign averages. (Right) The estimates  $\bar{n}_a$ .

When we plot the right-hand side of eq. (5.8) as a function of  $k_{\max}$ , we expect to observe a plateau. In the following, we choose the plateau region manually, and define  $k_{\max}$  to be the first point in the region. Note that  $\rho(m)$  and  $\tau_{\text{int}}$  depend on the choice of operators and replicas. We apply the above formulas to the operators  $f(z) = \text{Re}[e^{i\theta(z)}n(z)]$  and  $\cos\theta(z)$  at replica  $a = A$ . Note that these operators correspond to the real parts of the numerator and the denominator in (2.10).

We first investigate the autocorrelation for  $f(z) = \text{Re}[e^{i\theta(z)}n(z)]$ . Figure 8 shows the time series of  $\text{Re}[e^{i\theta(z)}n(z)]$ , and Fig. 9 shows  $\rho(m)$  as a function of  $m$ . We observe from

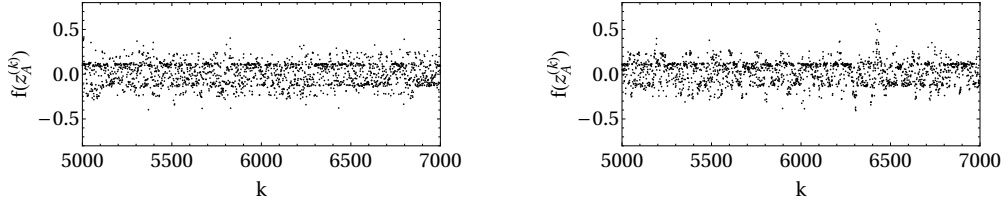


Figure 8: Histories of  $f(z_A^{(k)}) = \text{Re}[e^{i\theta(z_A^{(k)})}n(z_A^{(k)})]$  (with swap). (Left) HMC. (Right) Metropolis.

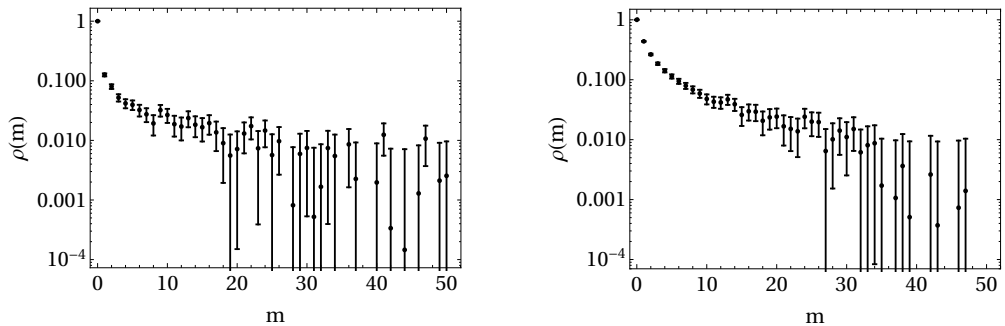


Figure 9: The normalized autocorrelation function for  $\text{Re}[e^{i\theta(z)}n(z)]$  (with swap). (Left) HMC. (Right) Metropolis.

Fig. 9 that  $\rho(m)$  decays faster for HMC, indicating smaller autocorrelation. We can confirm

this quantitatively from Fig. 10, where  $\tau_{\text{int}}$  is plotted as a function of  $k_{\text{max}}$ . The estimates of

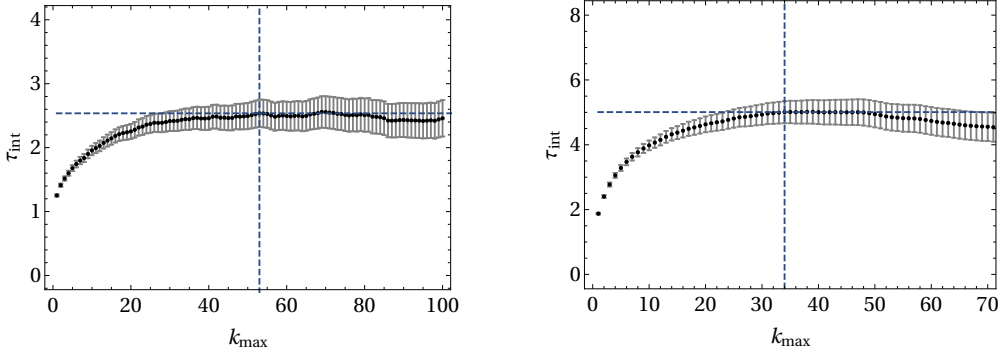


Figure 10: The estimates of  $\tau_{\text{int}}$  for  $\text{Re}[e^{i\theta(z)}n(z)]$  (with swap). (Left) HMC. (Right) Metropolis. The horizontal dashed line indicates the value of  $\tau_{\text{int}}$ , and the vertical dashed line indicates the value of  $k_{\text{max}}$ ,

$\tau_{\text{int}}$  are shown together with chosen values of  $k_{\text{max}}$  in Table 3. We see that  $\tau_{\text{int}}$  for HMC is

$f(z)$	algorithm	$\tau_{\text{int}}$	$k_{\text{max}}$
$\text{Re}[e^{i\theta(z)}n(z)]$	HMC	$2.54 \pm 0.21$	53
	Metropolis	$5.01 \pm 0.34$	34
$\cos \theta(z)$	HMC	$1.630 \pm 0.093$	24
	Metropolis	$3.53 \pm 0.23$	30

Table 3: The estimates of  $\tau_{\text{int}}$  (with swap).

about 50% of that for Metropolis with respect to this operator. A similar analysis is carried out for  $f(z) = \cos \theta(z)$  (see Figs. 11, 12 and 13). The estimates of  $\tau_{\text{int}}$  are shown in Table 3. We see that  $\tau_{\text{int}}$  for HMC is also about 50% of that for Metropolis with respect to this

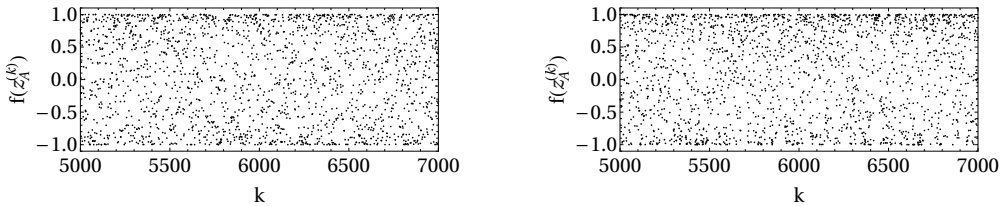


Figure 11: Histories of  $f(z_A^{(k)}) = \cos \theta(z_A^{(k)})$  (with swap). (Left) HMC. (Right) Metropolis.

operator.

As a comparison of the actual efficiency between two algorithms, we comment that the elapsed time to obtain a single configuration is in average 7.8 sec for HMC and 15 sec for Metropolis.<sup>23</sup> Therefore, the actual computational cost to obtain one independent config-

<sup>23</sup>The estimation was made by using Intel Xeon E5-2667 v4 running at 3.2 GHz with seven threads for each algorithm.

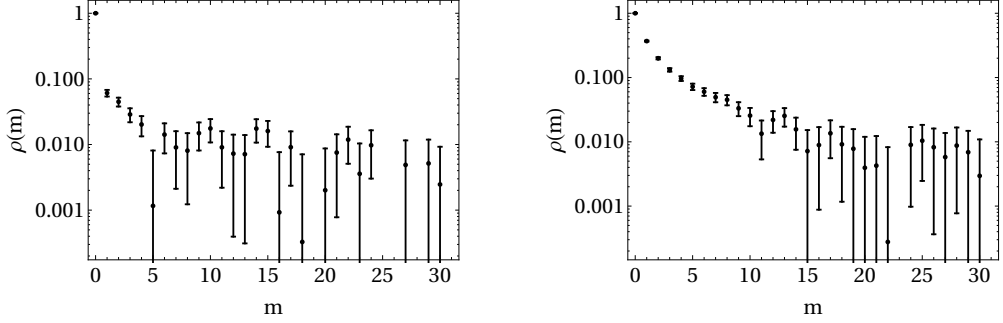


Figure 12: The normalized autocorrelation function for  $\cos \theta(z)$  (with swap). (Left) HMC. (Right) Metropolis.

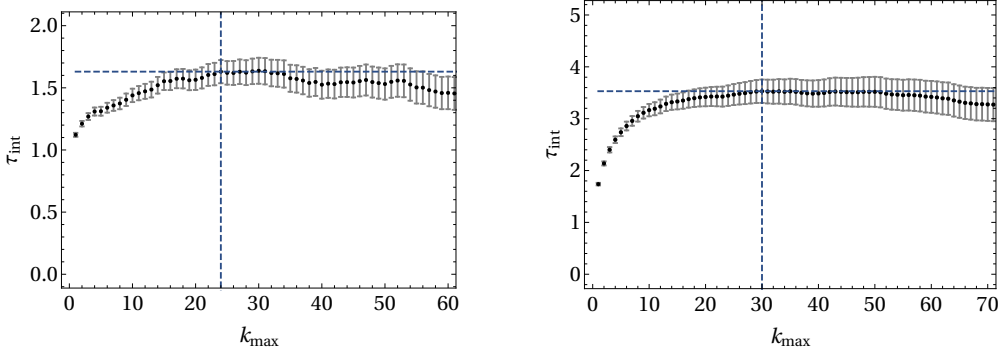


Figure 13: The estimates of  $\tau_{\text{int}}$  for  $\cos \theta(z)$  (with swap). (Left) HMC. (Right) Metropolis.

uration with HMC is about 30% of that with Metropolis. We expect that the benefits in computational cost become more significant as the degrees of freedom increase.

We here comment that the difference of  $\tau_{\text{int}}$  between HMC and Metropolis becomes more significant for simulations without swap. In Table 4 we summarize the results obtained without swap. The corresponding plots for  $f(z) = \text{Re}[e^{i\theta(z)}n(z)]$  are shown in Figs. 14, 15

$f(z)$	algorithm	$\tau_{\text{int}}$	$k_{\text{max}}$
$\text{Re}[e^{i\theta(z)}n(z)]$	HMC	$1.529 \pm 0.048$	7
	Metropolis	$11.5 \pm 1.0$	57
$\cos \theta(z)$	HMC	$1.340 \pm 0.033$	4
	Metropolis	$5.16 \pm 0.38$	41

Table 4: The estimates of  $\tau_{\text{int}}$  (without swap).

and 16, and those for  $f(z) = \cos \theta(z)$  in Figs. 17, 18 and 19. We see that  $\tau_{\text{int}}$  for HMC is 13 – 26% of those for Metropolis. The elapsed time to obtain a single configuration is in average 4.1 sec for HMC and 12 sec for Metropolis.<sup>24</sup> Thus the actual computational cost to

<sup>24</sup>The estimations were made with the same environment as footnote 23.

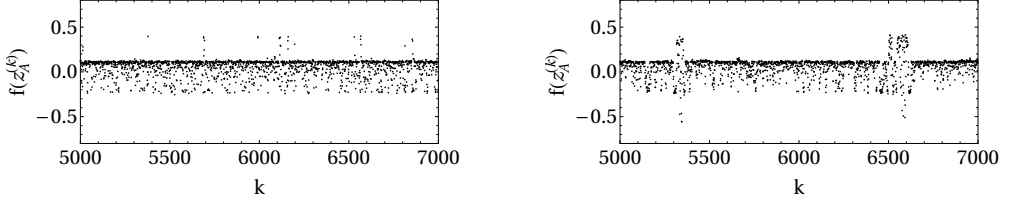


Figure 14: Histories of  $f(z_A^{(k)}) = \text{Re}[e^{i\theta(z_A^{(k)})}n(z_A^{(k)})]$  (without swap). (Left) HMC. (Right) Metropolis.

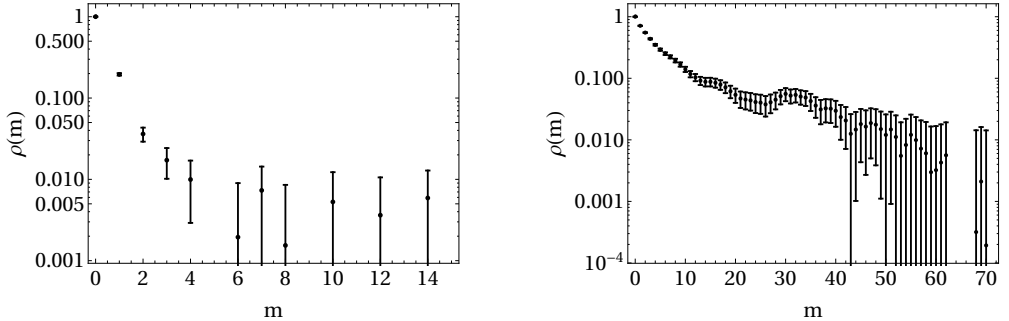


Figure 15: The normalized autocorrelation function for  $\text{Re}[e^{i\theta(z)}n(z)]$  (without swap). (Left) HMC. (Right) Metropolis.

obtain one independent configuration with HMC is less than 10% of that with Metropolis for the calculations without swap.

## 6. Conclusion and outlook

In this paper, we implemented the HMC algorithm on the TLTM, aiming to apply our algorithm to systems including fermions with large degrees of freedom. We observed that the actual computational cost to obtain an independent configuration becomes about 30% of that for the Metropolis algorithm even for small degrees of freedom ( $N = 20$ ).

We expect that the above improvement makes the TLTM more effective in solving the sign problems listed in Introduction, especially when performed on a large-scale computer. In parallel with the application of the algorithm to those problems (and also to some simplified model such as chiral random matrix models [35, 36]), it should be important to further develop the algorithm itself. In particular, the following three issues should be addressed:

- (1) It is desirable to have a systematic method to estimate numerical errors introduced in integrating the antiholomorphic gradient flow and in solving Newton's method iteratively (Step 1 in subsection 3.2).
- (2) We should investigate the scaling of computational cost as the degrees of freedom are increased. A simple estimate of the total cost of our algorithm is  $O(N^{3-4})$ .  $O(N^3)$  comes

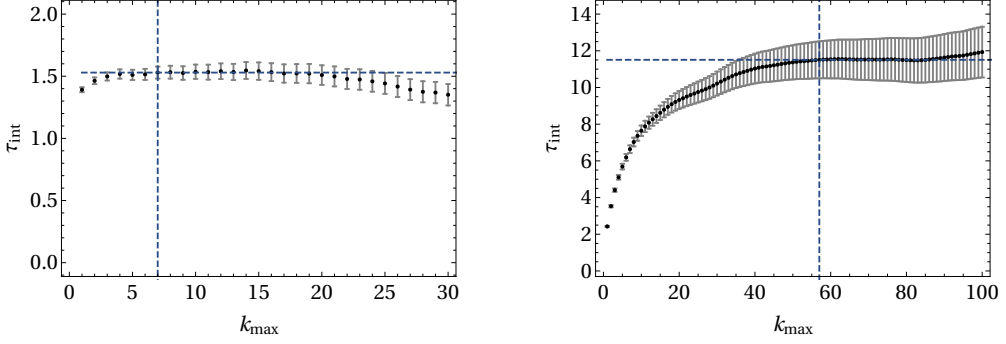


Figure 16: The estimates of  $\tau_{\text{int}}$  for  $\text{Re}[e^{i\theta(z)}n(z)]$  (without swap). (Left) HMC. (Right) Metropolis.

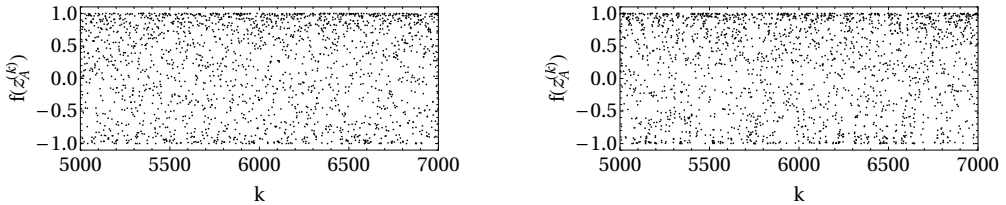


Figure 17: Histories of  $f(z_A^{(k)}) = \cos \theta(z_A^{(k)})$  (without swap). (Left) HMC. (Right) Metropolis.

from the calculation of the Jacobian, and  $O(N^{0-1})$  comes from the need to increase the number of replicas to keep the acceptance rates at swapping to significant values. It should be crucial to investigate if the above scaling is actually realized in large-scale calculations, because it then means that we can obtain correct results with a computational cost of a power of  $N$  (not exponentially).

(3) It should be helpful to have a systematic understanding of the *global sign problem* (i.e. cancellations of phases among different thimbles) and the *residual sign problem* (i.e. contributions from the phase factor  $e^{i\varphi(z)}$ ) for systems with large degrees of freedom, because they can be a cause of a significant increase of computational cost.

A study along these lines is now in progress and will be reported elsewhere.

## Acknowledgments

The authors thank Andrei Alexandru, Gerald Dunne, Hitotsugu Fujii, Yoshimasa Hidaka, Ken-Ichi Ishikawa, Issaku Kanamori, Masakiyo Kitazawa, Yoshifumi Nakamura, Yusuke Namekawa, Jun Nishimura, Akira Ohnishi, Yusuke Taniguchi and Shoichiro Tsusui for useful discussions, and especially Yoshio Kikukawa for sharing his insights on the RATTLE process in Lefschetz thimble methods. This work was partially supported by JSPS KAK-

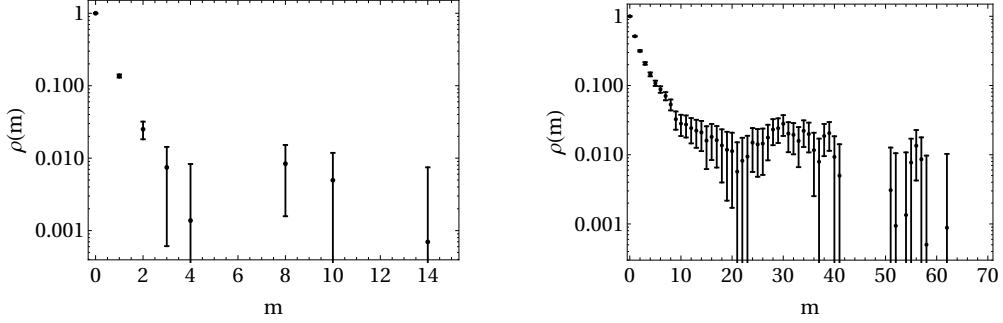


Figure 18: The normalized autocorrelation function for  $\cos \theta(z)$  (without swap). (Left) HMC. (Right) Metropolis.

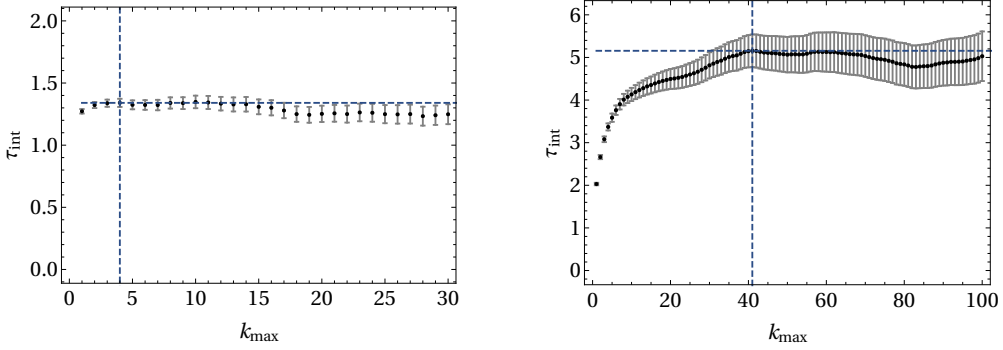


Figure 19: The estimates of  $\tau_{\text{int}}$  for  $\cos \theta(z)$  (without swap). (Left) HMC. (Right) Metropolis.

ENHI (Grant Numbers 16K05321, 18J22698 and 17J08709) and by SPIRITS 2019 of Kyoto University (PI: M.F.).

## References

- [1] G. Aarts, “Introductory lectures on lattice QCD at nonzero baryon number,” J. Phys. Conf. Ser. **706**, no. 2, 022004 (2016) [arXiv:1512.05145 [hep-lat]].
- [2] J. E. Hirsch, “Two-dimensional Hubbard model: Numerical simulation study,” Phys. Rev. B **31**, 4403 (1985).
- [3] E. Y. Loh, J. E. Gubernatis, R. T. Scalettar, S. R. White, D. J. Scalapino and R. L. Sugar, “Sign problem in the numerical simulation of many-electron systems,” Phys. Rev. B **41**, 9301 (1990).
- [4] M. Cristoforetti, F. Di Renzo and L. Scorzato, “New approach to the sign problem in quantum field theories: High density QCD on a Lefschetz thimble,” Phys. Rev. D **86**, 074506 (2012) [arXiv:1205.3996 [hep-lat]].

- [5] M. Cristoforetti, F. Di Renzo, A. Mukherjee and L. Scorzato, “Monte Carlo simulations on the Lefschetz thimble: Taming the sign problem,” *Phys. Rev. D* **88**, no. 5, 051501(R) (2013) [arXiv:1303.7204 [hep-lat]].
- [6] A. Mukherjee, M. Cristoforetti and L. Scorzato, “Metropolis Monte Carlo integration on the Lefschetz thimble: Application to a one-plaquette model,” *Phys. Rev. D* **88**, no. 5, 051502(R) (2013) [arXiv:1308.0233 [physics.comp-ph]].
- [7] H. Fujii, D. Honda, M. Kato, Y. Kikukawa, S. Komatsu and T. Sano, “Hybrid Monte Carlo on Lefschetz thimbles - A study of the residual sign problem,” *JHEP* **1310**, 147 (2013) [arXiv:1309.4371 [hep-lat]].
- [8] M. Cristoforetti, F. Di Renzo, G. Eruzzi, A. Mukherjee, C. Schmidt, L. Scorzato and C. Torrero, “An efficient method to compute the residual phase on a Lefschetz thimble,” *Phys. Rev. D* **89**, no. 11, 114505 (2014) [arXiv:1403.5637 [hep-lat]].
- [9] A. Alexandru, G. Başar and P. Bedaque, “Monte Carlo algorithm for simulating fermions on Lefschetz thimbles,” *Phys. Rev. D* **93**, no. 1, 014504 (2016) [arXiv:1510.03258 [hep-lat]].
- [10] A. Alexandru, G. Başar, P. F. Bedaque, G. W. Ridgway and N. C. Warrington, “Sign problem and Monte Carlo calculations beyond Lefschetz thimbles,” *JHEP* **1605**, 053 (2016) [arXiv:1512.08764 [hep-lat]].
- [11] M. Fukuma and N. Umeda, “Parallel tempering algorithm for integration over Lefschetz thimbles,” *PTEP* **2017**, no. 7, 073B01 (2017) [arXiv:1703.00861 [hep-lat]].
- [12] M. Fukuma, N. Matsumoto and N. Umeda, “Applying the tempered Lefschetz thimble method to the Hubbard model away from half filling,” *Phys. Rev. D* **100**, no. 11, 114510 (2019) [arXiv:1906.04243 [cond-mat.str-el]].
- [13] E. Witten, “Analytic continuation of Chern-Simons theory,” *AMS/IP Stud. Adv. Math.* **50**, 347 (2011) [arXiv:1001.2933 [hep-th]].
- [14] A. Alexandru, G. Başar, P. F. Bedaque and N. C. Warrington, “Tempered transitions between thimbles,” *Phys. Rev. D* **96**, no. 3, 034513 (2017) [arXiv:1703.02414 [hep-lat]].
- [15] S. Duane, A. D. Kennedy, B. J. Pendleton and D. Roweth, “Hybrid Monte Carlo,” *Phys. Lett. B* **195**, 216 (1987).
- [16] M. Creutz, “Global Monte Carlo algorithms for many-fermion systems,” *Phys. Rev. D* **38**, 1228 (1988).
- [17] H. C. Andersen, “RATTLE: A “velocity” version of the SHAKE algorithm for molecular dynamics calculations,” *J. Comput. Phys.* **52**, 24 (1983).
- [18] B. J. Leimkuhler and R. D. Skeel, “Symplectic numerical integrators in constrained Hamiltonian systems,” *J. Comput. Phys.* **112**, 117 (1994).

- [19] A. Alexandru, “Improved algorithms for generalized thimble method,” talk at the 37th international conference on lattice field theory, Wuhan, 2019.
- [20] A. Mukherjee and M. Cristoforetti, “Lefschetz thimble Monte Carlo for many-body theories: A Hubbard model study,” *Phys. Rev. B* **90**, no. 3, 035134 (2014) [arXiv:1403.5680 [cond-mat.str-el]].
- [21] Y. Tanizaki, Y. Hidaka and T. Hayata, “Lefschetz-thimble analysis of the sign problem in one-site fermion model,” *New J. Phys.* **18**, no. 3, 033002 (2016) [arXiv:1509.07146 [hep-th]].
- [22] M. Ulybyshev, C. Winterowd and S. Zafeiropoulos, “Taming the sign problem of the finite density Hubbard model via Lefschetz thimbles,” [arXiv:1906.02726 [cond-mat.str-el]].
- [23] M. Ulybyshev, C. Winterowd and S. Zafeiropoulos, “Lefschetz thimbles decomposition for the Hubbard model on the hexagonal lattice,” [arXiv:1906.07678 [cond-mat.str-el]].
- [24] R. H. Swendsen and J.-S. Wang, “Replica Monte Carlo Simulation of Spin-Glasses,” *Phys. Rev. Lett.* **57**, 2607 (1986).
- [25] C. J. Geyer, “Markov Chain Monte Carlo Maximum Likelihood,” in Computing Science and Statistics: Proceedings of the 23rd Symposium on the Interface, American Statistical Association, New York, p. 156 (1991).
- [26] K. Hukushima and K. Nemoto, “Exchange Monte Carlo method and application to spin glass simulations,” *J. Phys. Soc. Jpn.* **65**, 1604 (1996).
- [27] Y. Saad and M. H. Schultz, “GMRES: A Generalized minimal residual algorithm for solving nonsymmetric linear systems,” *SIAM J. Sci. and Stat. Comput.* **7**, 856 (1986).
- [28] H. A. van der Vorst, “Bi-CGSTAB: A fast and smoothly converging variant of Bi-CG for the solution of nonsymmetric linear systems,” *SIAM J. Sci. and Stat. Comput.* **13**, 631 (1992).
- [29] A. Alexandru, G. Basar, P. F. Bedaque and G. W. Ridgway, “Schwinger-Keldysh formalism on the lattice: A faster algorithm and its application to field theory,” *Phys. Rev. D* **95**, no. 11, 114501 (2017) [arXiv:1704.06404 [hep-lat]].
- [30] Y. Sugita and Y. Okamoto, “Replica-exchange molecular dynamics method for protein folding,” *Chem. Phys. Lett.* **314**, 141 (1999).
- [31] M. Fukuma, N. Matsumoto and N. Umeda, “Distance between configurations in Markov chain Monte Carlo simulations,” *JHEP* **1712**, 001 (2017) [arXiv:1705.06097 [hep-lat]].
- [32] M. Fukuma, N. Matsumoto and N. Umeda, “Emergence of AdS geometry in the simulated tempering algorithm,” *JHEP* **1811**, 060 (2018) [arXiv:1806.10915 [hep-th]].

- [33] M. B. Priestley, “Spectral analysis and time series,” Academic Press, London (1981).
- [34] N. Madras and A. D. Sokal, “The pivot algorithm: A highly efficient Monte Carlo method for self-avoiding walk,” *J. Statist. Phys.* **50**, 109 (1988).
- [35] M. A. Stephanov, “Random matrix model of QCD at finite density and the nature of the quenched limit,” *Phys. Rev. Lett.* **76**, 4472 (1996) [hep-lat/9604003].
- [36] A. M. Halasz, A. D. Jackson, R. E. Shrock, M. A. Stephanov and J. J. M. Verbaarschot, “On the phase diagram of QCD,” *Phys. Rev. D* **58**, 096007 (1998) [hep-ph/9804290].